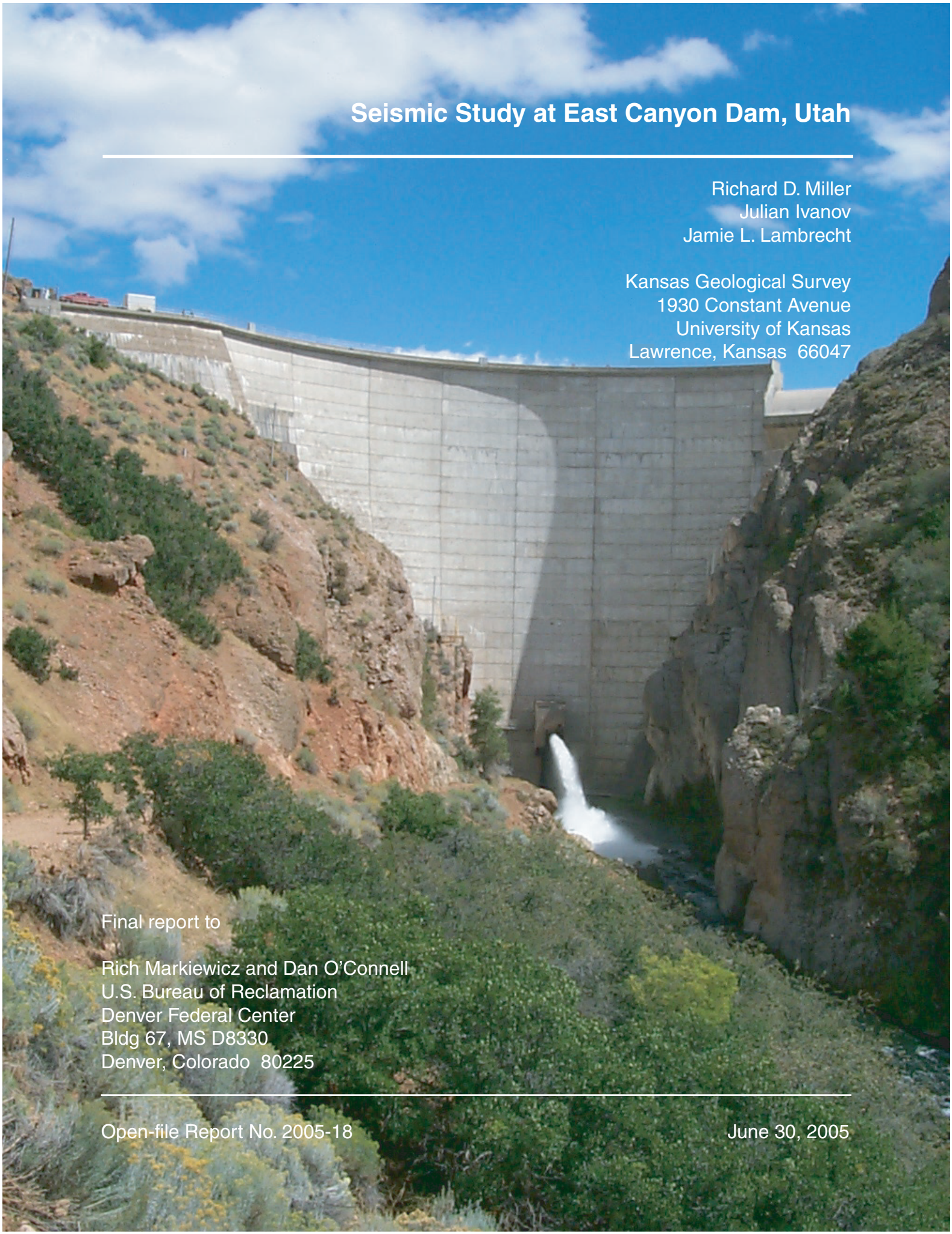

Seismic Study at East Canyon Dam, Utah

Richard D. Miller
Julian Ivanov
Jamie L. Lambrecht

Kansas Geological Survey
1930 Constant Avenue
University of Kansas
Lawrence, Kansas 66047

Final report to

Rich Markiewicz and Dan O'Connell
U.S. Bureau of Reclamation
Denver Federal Center
Bldg 67, MS D8330
Denver, Colorado 80225

Open-file Report No. 2005-18

June 30, 2005

Seismic Study at East Canyon Dam, Utah

Richard D. Miller
Julian Ivanov
Jamie L. Lambrecht

Kansas Geological Survey
1930 Constant Avenue
University of Kansas
Lawrence, Kansas 66047

Final Report to

Rich Markiewicz and Dan O'Connell
U.S. Bureau of Reclamation
Denver Federal Center
Bldg 67, MS D8330
Denver, Colorado 80225

Seismic Study at East Canyon Dam, Utah

Executive Summary

A reliable measure of seismic properties as a function of depth is important to the U.S. Bureau of Reclamation's comprehensive and accurate appraisal of site response and vibration modes in the thin concrete arch East Canyon Dam in Morgan County, Utah. This applied research project measured in-situ compressional and shear velocities using VSP methods, attempted to map the 2-D compressional- (using turning-ray tomography [Ivanov, 2002]) and shear-wave (Miller et al., 1999) velocity field along the toe road and across the crest of the dam, measured compressional- and shear-wave frequency response as a function of amplitude at a point within the dam, at the concrete/rock interface, and in the rock, and mapped events (possibly reflectors) within the upper 350 ft using high-resolution compressional- and shear-wave seismic reflection techniques (Steeples and Miller, 1990). Seismic reflection profiles were designed to provide information concerning the consistency and geometry of layering between boreholes and identify anomalies (within the upper 350 ft and 1000 ft upstream and downstream) that might influence realizations. These measurements of velocity and maps of bed geometry were acquired to support the more general sitewide characterization underway by the Bureau of Reclamation.

Complexity of the geologic features at this site inhibited confident pre-survey determination as to how well and if any of the routine geophysical techniques for measuring velocity and mapping variability in the near-surface velocity field would provide meaningful data for incorporation with downstream ground motion simulations. A necessary objective of this applied research project was to evaluate the effectiveness of coincident measurements of in-situ compressional and shear velocities using checkshot, VSP, MASW (Park et al., 1999), turning-ray tomography (Zhang and Toksoz, 1998), and high-resolution seismic reflection (Steeples and Miller, 1990). All these methods and associated measurements were focused on rocks within 350 ft of the ground surface. Compressional-wave velocity cross-sections from tomography at the toe correlate extremely well with outcrop and reflection data. MASW data from the toe were consistent with the borehole-measured shear-wave velocity and tomography cross-sections processed for the toe line.

Compressional- and shear-wave high-resolution seismic reflection surveys allowed very crude interpretations of near-surface geometries, which were correlated with moderate confidence to what was known about the local geology. Seismic reflection is a technique that is hampered by an extremely irregular geologic setting, such as this one. Dipping layers, highly fractured rocks with several major facture orientations, rocky and irregular near-surface material, unsorted and very attenuative conglomerate rocks, and steep out-of-the-plane cliff faces are all physical characteristics of this site that make using shallow, high-resolution seismic reflection extremely challenging. A combination of indirect evidence (localized scatter events, lateral changes in apparent velocity, changes in signal-to-noise, etc.) and geologic data (borehole measurements and samples, outcrop studies, local setting, etc.) incorporated with the interpretable primary reflected energy arrivals allow an estimation of the gross seismic characteristics and associated geologic features along these CMP profiles.

Any measurement of velocity and interpretation of bed geometry provides important complementary data for the ongoing Bureau of Reclamation site characterization. The more

accurate and laterally complete the complementary seismic measurements the more representative the ground motions simulations. Seismic reflection profiles were used to provide information concerning the consistency, extent, and geometry of layering between boreholes and identify lateral variations (within the upper several hundred feet extending about 300 ft upstream and around 1500 ft downstream) that might influence realizations. Based on several assumptions it appears the high-velocity conglomerate is about 500 ft thick at the dam along the right abutment and thins to about 350 ft thick at the toe where it thickens to about 500 ft about 400-800 ft from the outlet. From 400-500 ft west of the outlet the conglomerate thins rapidly to depths below resolution limits.

Borehole velocity measurements were made in two boreholes—one on the dam crest and one downstream. The unique receiver system provided by the Geological Survey of Canada incorporates three independent pods, each with three sensors polarized to record a different component of the wave field. VSP data were acquired and processed in a fashion to facilitate the measurement of compressional and shear velocities throughout the drilled intervals, specifically taking advantage of the fixed separation between pods for improved estimations of interval velocities. Accuracy of the measured velocity was dependent on the consistency of the source wavelet and coupling of the receiver to the borehole walls. Borehole coupling is critical for optimal interfacing with engineering studies of the dam and incorporation with sonic data acquired using standard wireline logging equipment and techniques. With longitudinal and transverse oriented shear-velocity measurements, it is possible to identify zones within the borehole possessing shear-wave anisotropy. However, fracture zones in this geologic setting make it difficult to distinguish anisotropy from poor receiver coupling especially if the directionally dependent differences are expected to be subtle.

The two boreholes were drilled with different targets and specific objectives. The downstream boring (immediately west of the outlet works) targeted near-surface sediments and helped to establish trends/consistency in material properties away from the structure. A deeper boring placed on the dam crest sampled about 53 ft of the dam thrust block and another 350 ft or so of the natural foundation material. The entire portion of the native materials sampled in these boreholes was the conglomerate observed in outcrop. Two pronounced areas with anisotropy and two areas with velocity inversions were identified in the crest well. Fractured rock is prevalent, causing significant scatter of seismic energy. Correlations between the toe and crest boreholes were not made with great confidence, but some inference can be made about the possible depth to the basal contact from the VSP data.

Coincident with but independent of the surface seismic program originally proposed and carried out by the KGS was seismic response analysis of the dam involving an acentric vibrator dwelling at specific frequencies and recording response characteristics along the crest of the dam. Data recorded within the dam, at the dam/rock interface, and in the rock using the three component, three pod borehole receiver as a function of frequency were used to establish empirical characteristics of the dam/rock interface as it relates to the transmission of seismic energy, specifically shear energy.

Seismic Study at East Canyon Dam, Utah

Summary

Compressional- and shear-wave reflection, compressional and shear VSP/check shot, compressional-wave refraction tomography, and multichannel analysis of surface waves (MASW) techniques were evaluated and determined to be marginally effective and reasonably accurate, and subsequently used to improve our understanding of the seismic-wave velocity structure of rocks supporting a thin-arch concrete* dam in north-central Utah. A reliable measure of seismic properties as a function of depth is an important component in a comprehensive and accurate appraisal of site response and vibration modes in concrete dams. Models used to predict dam performance during earthquakes are only as realistic as the material attributes incorporated into those simulations. Proven correlation between seismic properties and stiffness/rigidity is the basis for making highly detailed measurements of the seismic wavefield at developed or to-be-developed sites. Optimal 30-fold CMP seismic reflection profiles provided gross images of the massive conglomerate supporting the dam and uniformly present in outcrop around the dam. The conglomerate possesses bedding plains dipping upward of 20 degrees and visible fractures both along bedding plains and at oblique angles to dominant bedding surfaces. Of particular interest was the right abutment of the dam, which was the area with rocks most accessible to study and represented the area with the strongest potential influence on the dam performance during a ground-shaking event at this site. VSP profiles in boreholes installed through both the concrete dam and downstream toe provided velocity control and identified changes in rock properties within 250 ft of the ground surface. Energy partitioning and associated changes in frequency, amplitude, and mode of seismic energy appears quite pronounced at the concrete/rock interface of the dam. Continuous, detailed, coincident measurements of compressional- and shear-wave velocities throughout the geologic section were acquired and should be of sufficient quality to be included in realizations of site response to determine if this structure has failure potential in this seismic risk area.

Introduction

A reliable measure of seismic properties as a function of depth is important to the U.S. Bureau of Reclamation's comprehensive and accurate appraisal of site response and vibration modes in the thin concrete arch East Canyon Dam in Morgan County, Utah (Figure 1). Material response to shaking within and in proximity of the dam must be reasonably well known for accurate estimation of failure potential and associated risk. Any significant ground motion at this dam site will likely be controlled or at least influenced by an unnamed fault less than 300 ft upstream of the dam structure or the Wasatch Fault, about 12 miles west of the dam. Models used to predict dam performance during earthquakes and floods

Figure 1. East Canyon Dam.

*Cement binds the aggregate together in concrete.

are only as realistic as the material attributes (especially rigidity) incorporated into those simulations. Proven correlation between seismic properties and stiffness/ rigidity were the basis for highly detailed measurements of the seismic wavefield at this dam site. Realizations for areas with liquefaction or rock failure potential are enhanced when the velocity field used to calculate Poisson's ratio is based on representative, continuous, detailed, coincident measurements of compressional and shear-wave velocities at each significant geologic contact and within each major geologic unit.

East Canyon Dam

Text removed at request of BoR security personnel.

(Figure 2)
(Figure 3)

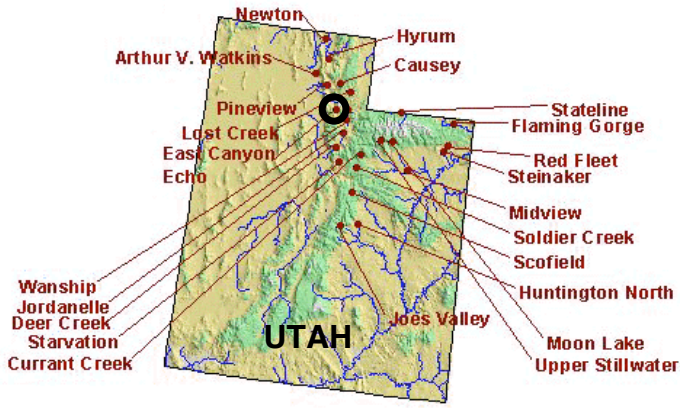

Figure 2. Utah Bureau of Reclamation dams.

Figure 3. East Canyon Dam. Red truck on far right side of dam (left/right convention relative to looking downstream).

(Figure 4). Completed in 1966, it is located in a narrow-walled canyon where the East Canyon Creek has cut through very hard, massive, well-cemented beds of late upper Cretaceous conglomerate (Figure 5). This massive conglomerate is part of a sequence of layers possessing a dominant upstream dip. In outcrop this conglomerate rock body is dominated by fracture systems aligned with as well as at oblique angles to exposed bedding planes. Characteristic of these kinds of massive conglomerate bodies are layers and lenses of unsorted material from clay to boulder size (Figure 6). Zones

Figure and caption removed at request of BoR security personnel.

Figure 4.

Figure 5. View of conglomerate rock, which is the foundation for the dam.

Figure 6. Rock outcrop along toe road. Unsorted and variable grain size of the conglomerate are evident in most exposures. Seismic energy propagation is severely disturbed by irregularities in material properties and discontinuities in the rocks.

of weakly cemented rock fragments appear in outcrop scattered around this site. Considering the seismicity of this area, seismic and structural characteristics of the dam and the upper 300 to 400 ft of sediments supporting the dam will dictate how the dam responds to ground motion.

Methods

This project attempted to evaluate the applicability of several seismic techniques to identify, delineate, and estimate the seismic characteristics or properties of materials within and beneath East Canyon Dam. These methods include: P-wave refraction tomography (2-D turning ray), surface-wave analysis (MASW), VSP (near-vertical and offset), checkshot survey (downhole), spectral analysis, and 2-D P & S reflection.

- Turning-ray tomography was used to define Vp for subsurface cells along the 2-D profiles acquired at the crest and toe of the dam targeting velocity variations within the near-surface rock, joints/ fractures within the shallow rock layers, and characteristics of the rock/concrete interface.
- Compressional- and shear- (oriented both longitudinal and transverse) wave near-vertical and offset VSP surveys were conducted in two holes (one at the crest through the concrete dam and several hundred feet into the right abutment rock and one through the native conglomerate rock at the toe of the dam). Primary objectives of the VSP surveys were to identify and delineate the basal contact of the conglomerate the dam is built on and extrapolate the measured velocity structure encountered in the boreholes to locations away from the boreholes.
- Check-shot survey (downhole velocity survey) was designed to acquire average and interval velocities within the concrete dam and conglomerate, looking specifically at anomalous zones and velocity anisotropy effects.
- Multichannel analysis of surface wave (MASW) inversion techniques focused on shear-wave velocities within the upper few tens of feet of the conglomerate at the toe and within the concrete portion of the dam and the contact between the dam and rock. Specifically the survey along the crest was attempting to identify anomalies that might be present within a thin zone at the contact between the dam and native rock.

- Compressional- and shear-wave, 2-D high-resolution seismic reflection data were acquired along the right abutment and at the toe perpendicular to the axis of the dam. The surveys were designed to evaluate the feasibility of and, if feasible, proceed coincidently mapping changes in rock properties as indicated by changes in Vp and Vs. A key target was delineating the basal contact of the conglomerate and defining its geometry as far upstream as possible and at least 1000 ft downstream of the dam.
- Simultaneous analysis of the response of the concrete dam, native rock, and contact between the rock and concrete at specific frequencies was accomplished using a surface-mounted vibrator and three three-component downhole receivers. Full wavefield measurements were made at specific frequencies and at constant amplitudes on the dam crest. An acentric vibrator was used to generate predominantly shear-wave energy that was measured at the contact, in the concrete 6.5 ft above the contact, and in the conglomerate 6.5 ft below the contact.

Each of these methods was applied at locations and in a fashion appropriate for the method (Figure 7). Tests were designed to measure key seismic characteristics and/or properties as well as determine field efficiency, resolution potential, interpretability (signal-to-noise), processing requirements, consistency with ground truth (accuracy), and measurement confidence (especially as to the relational nature of the characteristics/properties as determined by the various methods used here and other supporting data, such as wireline logs), which are integral properties of the individual seismic technique studies.

Reflection

High-resolution seismic reflection surveys included both compressional- and shear-wave modes. It was hoped the seismic reflection data quality would be sufficient to delineate the 2-D geometry of the conglomerate along the right abutment road and toe road. If numerical vibration models are to be constructed using seismic reflection interpretations, a great deal of confidence that the reflection-derived interpretations are representative of the shallow earth material is necessary to accurately depict the response of this massive conglomerate/dam system under various levels of potential ground motion. An ancillary objective of the reflection surveys was to extend the Vp/Vs relationship within the conglomerate as far as possible upstream and down-stream along the right abutment. The geometry and velocity structure of the massive conglom-erate that the dam is constructed on are essential components of vibration models and associated simulations used to evaluate the resistance/susceptibility of the structure to failure due to earthquake energy.

Preliminary estimates suggested a properly designed and executed high-resolution P-wave or S-wave seismic reflection survey should be capable of mapping all reflectors with reflectivity of at least 0.5 (e.g., clay/gravel) and separated by 20 ft or more within the interval of interest at the East Canyon Dam site. To maximize our potential for success, meeting those objectives we concentrate on: 1) generating and recording high frequency (> 120 Hz P-wave and > 60 Hz S-wave) signals; 2) optimizing spread deployment and acquisition for 2-D imaging of dipping beds and low reflectivity contacts; 3) establishing the best configurations and parameters to maximize signal-to-noise and resolution potential at this site; 4) correlating P-wave reflections with S-wave reflections as well as with VSP and drill data; 5) ensuring offset distributions were appropriate for estimating velocity from NMO curves and correlating those to average-velocity

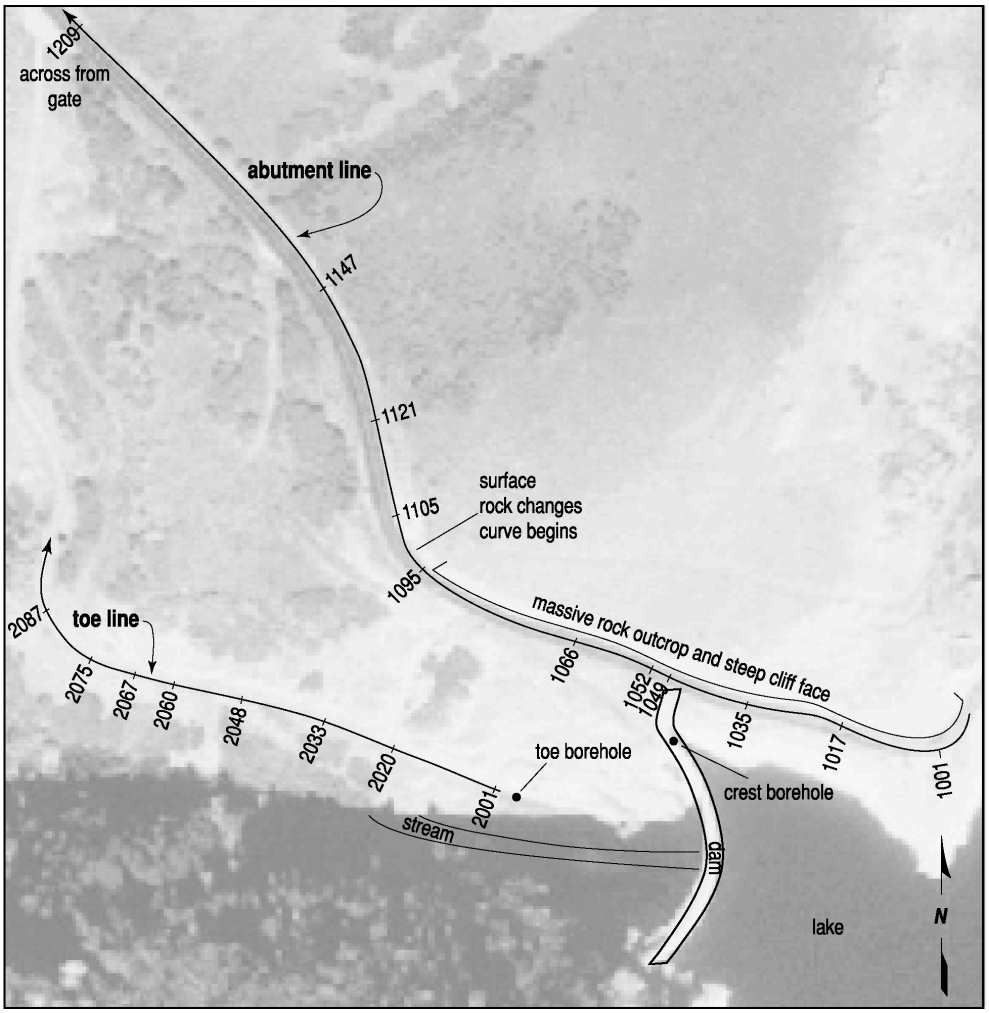

Figure 7. Site map at East Canyon Dam showing the seismic lines, station numbers, physical descriptions, dam and lake locations, and borehole locations superimposed on an aerial photo.

curves from VSPs; 6) integrating well-established shallow high-resolution methodologies and conventional approaches; 7) tailoring processing flows to optimize the accuracy and spatial distribution of velocity analysis for most accurate Vp/Vs; and 8) correlating polarized shear-wave velocities from CMP with oriented and polarized Vs measured in the boreholes. Proven high-resolution techniques were used in designing the data acquisition parameters and determining optimum equipment and methodologies (Steeples and Miller, 1990).

Maximizing the resolution potential, interpretability, and signal-to-noise ratio was emphasized throughout the reflection component of this study. Continuous CMP profile lines (Mayne, 1962) were acquired along the right abutment using a 216-channel fixed spread and an 84-channel spread for the toe line. Traces outside the optimum recording window for each recorded shot were deleted during processing (Hunter et al., 1984). The seismic source, geophone type, spread geometry, shots/point, and acquisition philosophy used to acquire the CMP profile lines were based on the results of walkaway noise tests and preliminary on-site analysis of VSP data and MASW/tomography data. Reflection data were acquired and processed to

delineate local stratigraphic, structural, and topographic features within the upper 1000 ft using state-of-the-art high-resolution methodologies and equipment.

Refraction/Tomography

Direct and refracted first-arriving P-wave energy were analyzed using inversion techniques (Scott, 1977; Schneider et al., 1992; Zhang and Toksoz, 1998). Use of direct and refracted arrivals for mapping distinct velocity contrasts between layers has been in routine use for everything from crustal seismic research (Steinhart and Meyer, 1961) to shallow groundwater studies (Haeni, 1978). It is an established, proven technique whose limitations are well documented (Soske, 1954; Sander, 1978). Methods have been developed and proven to approximate solutions when physical conditions violate the basic assumptions of the refraction method (Palmer, 1980; Mooney, 1981; Redpath, 1973). Recent research incorporating refraction inversion with shear-wave velocity calculations from surface-wave data has provided encouraging results that seem to be insensitive to the most significant problems: velocity reversal and nonuniqueness (Ivanov, 2002).

Tomography has been used throughout the industry for a variety of subsurface applications, including: waste repository characterization (Peterson et al., 1985), engineering studies (Cottin et al., 1986), void detection (Lytle and Dines, 1980), and mining (Kilty and Lange, 1990). The simplicity of acquisition and computational intensity makes it especially applicable for velocity estimation using data acquired for surface-wave and/or refraction analysis. Using this approach in conjunction with multichannel surface-wave inversion, anomalous features within the dam can be examined while studying the very shallow velocity structure at and above the boundary between the weathered and unweathered layers. Correlation to borehole-derived compressional- and shear-wave data can help accurately constrain estimates of models during inversion. Data processed for tomographic analysis used proven algorithms and a standard curved-ray approach (Zhang and Toksoz, 1998).

Surface Wave Inversion (MASW)

Surface waves traditionally have been viewed as noise in multichannel seismic data collected to image targets for shallow engineering, environmental, and groundwater purposes (Steeples and Miller, 1990). Recent advances in the use of surface waves for near-surface imaging have combined spectral analysis techniques (SASW), developed for civil engineering applications (Nazarian et al., 1983), with multi-trace reflection technologies developed for near-surface (Schepers, 1975) and petroleum applications (Glover, 1959). The combination of these uniquely different seismic approaches to imaging the shallow subsurface permits reasonably accurate (±10%) non-invasive estimation of shear-wave velocities (Xia et al., 2002) and delineation of horizontal and vertical variations in near-surface material properties based on changes in these velocities (Park et al., 1996; Xia et al., 1999; Park et al., 1999).

A 2-D continuous shear-wave velocity profile of the subsurface results when these techniques are integrated. This highly redundant surface-wave method is a clear advancement over traditional two-receiver methods because of its improved accuracy of calculated shear-wave velocities and it minimizes the likelihood that irregularities resulting from erratic dispersion curves will corrupt the analysis. Surface-wave analysis was performed on data recorded along the crest and at the toe of the dam (Figure 7). Both profiles were acquired using the accelerated weight drop and 30-receiver towed array.

Downhole/VSP

Borehole seismic measurements allowed checkshot-style downhole measurements as well as vertically incident and offset VSP analysis. Borehole data were acquired and processed to provide compressional and shear velocities throughout the drilled intervals, mindful of the needs of the engineering studies these data were acquired to complement for the dam. Both longitudinal- and transverse-oriented shear velocity measurements were acquired to identify and map any significant shear-wave anisotropy within the boreholes.

Two boreholes were drilled at East Canyon Dam for the study with similar yet unique objectives (Figure 7). Data acquired in the toe (downstream) borehole targeted the shallower near-surface sediments (< 250 ft) and were intended to help establish trends/consistency in material properties downstream of the dam foundation. A deeper boring on the dam crest was positioned to sample about 55 ft of the dam's thrust block and another 350 ft or so of the natural foundation material. Preliminary models suggested a 400 ft deep boring should penetrate the basal contact of the conglomerate exposed at the ground surface. Once beneath the concrete dam, the drill bit encountered native material (conglomerate observed in outcrop) throughout the 400 ft sampled interval.

Surface-to-borehole data were acquired to determine the 3-C velocity field as a function of depth. Acquisition, processing, and interpretation of vertical seismic profiles (VSP) followed well-established guidelines (Hardage, 1983). As with most seismic methods, adapting methodologies developed in the oil industry to shallow targets requires deviating from accepted "rules of thumb." An offset VSP was acquired with the source offset (115 ft crest hole and 100 ft toe hole) along the proposed reflection line at the toe and north parallel to the crest at the crest hole. Near-vertical offset VSP (ZVSP) provided the best measure of average velocity as a function of depth. Offset VSP (OVSP) profiles are best suited to help with lithologic and structural interpretation of reflection profiles. VSP sections are processed and interpreted so reflectors intersecting the borehole can be mapped radially away from the borehole to a maximum offset of about one-quarter the borehole depth (70 ft to 80 ft in this case). For data acquired during this survey, the complexity in energy arrivals precluded corridor stacking.

Acquisition

Five data acquisition methods were used during this study (shear-wave CMP, compressional-wave CMP, MASW, turning-ray tomography, VSP/check shot, and frequency-amplitude monitoring). Seismic sources included an IVI minivib 1 in both compressional and shear configurations, an acentric vibrator, and an accelerated weight drop. The seismograph used for all components of this study was a 240-channel, Geometrics StrataView w/NZC StrataVisor* (Figure 8). While acquiring borehole data only 9 channels were active, for CMP data acquisition 216 channels were active for the right abutment line and 84 for the toe line, and for MASW and tomography towed-spread data 30 channels were active. Receivers used during this study included single Geospace 4.5 Hz vertical geophones wired in series for the tomography and MASW, a pair of Mark Products 40 Hz geophones for the compressional-wave reflection acquisition, single Geospace 14 Hz horizontal geophones for recording the shear-wave

*Trade names, trademarks, and service marks are the property of their respective owners, and are given here for information purposes only. No endorsement is given or implied by the Kansas Geological Survey or the U.S. Bureau of reclamation of any project or service.

Figure 8. Geometrics StrataView 240-channel seismograph w/NZC StrataVisor controller mounted on a 6-wheel John Deere Gator ATV.

Figure 9. Shear geophone (blue) planted with compressional geophones (red) at a typical location along toe road.

reflection data, and a custom designed three-pod, three-component Geostuff hole lock geophone system for all borehole recording (Figure 9).

Surface Seismic Reflection

Seismic reflection profiles included a compressional- and shear- (SH) wave survey along the right abutment road and along the toe road (Figure 7). The toe-road line started near the outlet works and proceeded west along the road, halting at the abrupt north curve approximately 900 ft from the dam. Receiver spacing was 8 ft and source spacing was 16 ft for both modes and locations. Along the abutment line a total of just over 1600 ft of profile was acquired starting near the lake/dam overlook, immediately northeast of the dam, to just below the gate accessing the outlet (Figure 10). Geophones were planted in the north-road shoulder in a very loose, unsorted rubble material making good receiver coupling difficult and coupling in general very inconsistent from station to station (Figure 11). Single shear-wave geophones were oriented to match the polarized shear energy

Figure 10. View west approximately in the center of the abutment reflection line. Traffic was restricted to one lane during data acquisition.

Figure 11. Geophones were planted in loose gravels along the north-road shoulder. Coupling was generally poor and inconsistent.

Figure 12. Vibrator setup at station downstream of dam along right abutment road. Receivers and cables in north road ditch.

Figure 13. Vibrator setup on toe road with rock ledges both north and south of road. Seismograph vehicle set up to allow vibrator to move past during acquisition. Receivers are along north side of road.

produced by the vibrator (Figure 9). A fixed 216-receiver spread geometry recorded all sweeps as the source rolled through the line (Figure 12). The resulting offset distribution is symmetric about the center of the spread with a maximum offset that ranged from around 1750 ft to 860 ft and an average minimum offset of around 6 ft. Toe-road reflection recording for both P- and S-wave data required 84 recording channels and included about 680 ft of profile. Receivers were located in the north-road shoulder at the base of the rock ledge for both toe data sets (Figure 13).

Sources

Seismic sources for the various data sets recorded included the IVI minivib 1 (Figure 14), Rubber band Assisted Weight Drop (RAWD) (Figure 15), and the Bureau of Reclamation's acentric vibrator (Figure 16). Each source was tuned for the site conditions and requirements of the survey. For borehole work the vibrator was used to generate shear-wave energy and the weight drop produced all compressional energy (Figure 17). [Sentence removed at request of BoR security personnel] (Figure 18). Recording data from the acentric vibrator was piggybacked onto experiments being carried out independently by Bureau of Reclamation researchers.

Figure 14. IVI minivibI in SH mode along abutment.

Figure 15. Case loader operating RAWD and towing streamer (spread).

Figure removed at request
of BoR security personnel.

Figure 16. Acentric vibrator bolted to dam crest. Weights are added to spinning arms to change amplitude.

Figure 17. Vibrator and RAWD equidistant from toe borehole. Vibrator was producing shear energy and weight drop was providing compressional.

Figure and caption removed at request
of BoR security personnel.

Figure 18.

For the non-reflection data sets compressional-wave energy was generated with the accelerated weight drop (RAWD), which is a KGS design incorporating principles of Bison's elastic-wave generator with several components from agricultural equipment (Figure 19). The RAWD used on this project accelerates a 150 lb mass using a rubber band to produce 1660 N of force and 668 Joules of energy. Powering the RAWD is a Case skid-steer loader equipped with an electric winch for extending and retracting the land streamer after the streamer is positioned at the appropriate spread location (Figure 20).

The use of vibratory sources increases the potential for spectral shaping of the recorded wavelet, minimizes the environmental impact for a given amplitude source wavelet, and increases the signal-to-noise ratio, while increasing the complexity of in-field and/or post-acquisition processing when compared to non-coded impulsive sources. Vibratory techniques were first developed over 40 years ago as an alternate method (non-impulsive) of introducing acoustic energy into the ground (Crawford et al., 1960). This oscillatory energy method known as "vibroseis" uses a controlled vibrating source to generate a sinusoidal wavetrain of continuously varying frequency delivered to the ground over a specific time period (Sheriff, 1991).

Figure 19. Case loader with RAWD attached to loader arms. Hydraulic power is provided by the loader.

Figure 20. Case loader towing the streamer with cable attached to an electric winch to allow quick changes in source offset.

The sweep (sinusoidal source input function) trace, or pilot, is correlated with each recorded time series trace. The record time of each data trace is slightly longer than the sweep (pilot) time to allow sufficient "listen" time for two-way travel of the entire sweep energy. The correlation process effectively produces a time-series trace comparable to impulsive-source records with respect to full-wave field recording.

The IVI minivib was used in compressional-wave mode and then switched on site to shear (Figure 21) as needed for the surface reflection and borehole data acquisition. The source was pressure coupled to the asphalt road, dam crest, and gravel toe road using the weight of the vibrator (14,000 lbs). A neoprene liner on the bottom of the baseplate was in direct contact with the road surface for both compressional and shear configurations. The waffle plate configuration (Figure 22) was not used to avoid road damage and to increase the coupling area. Visual inspection of the vibrator pad locations immediately following vibration indicates no road surface damage was caused by any of the vibration testing.

Figure 21. Vibrator pad with mass oriented transverse to line direction and center line of vehicle.

Figure 22. Waffle plate (blue) traditionally used to couple the baseplate to ground surface. Damage and lost coupling precludes its use on paved roads.

Optimum sweeps used for the two survey types (borehole and surface) were determined after on-site testing. All sweeps were linear up-sweeps with a 1 second front taper and 0.25 end taper. Both longitudinal and transverse shear-wave energy recorded for the borehole VSP was produced using the vibrator. Sweep length for the borehole data was 3.5 seconds with a sweep frequency range of 10 Hz to 150 Hz. All borehole data were recorded with a .25 ms sampling interval and 4-second record length. For the surface reflection data, unique sweep parameters were used for shear- and compressional-wave energy recording. For the shear data a 10 Hz to 150 Hz, 10-second sweep was used with a 12-second recording time, 1 ms sampling interval, and source and receivers polarized in an SH orientation. Sweep frequencies for compressional-wave reflection data were 10 seconds long and included frequencies from 25 Hz to 250 Hz recorded over 12 seconds with a 1 ms sampling interval.

All vibrator data were recorded uncorrelated, allowing maximum flexibility during processing to enhance data "correlation." Mass- and baseplate-accelerometer data were recorded for each sweep. These data were used to produce a ground-force trace which, when compared with the ideal or synthetic drive signal, provided a reasonable indicator of energy transfer efficiency. Both types of pilot traces were tested using correlation and deconvolution routines. This testing was intended to establish which was the optimum method for compressing these frequency-variable time series traces into broadband impulsive source wavelets. If a true "ground force" (actual time series representation of the seismic energy propagating from the source) could be measured or calculated, theory predicts deconvolution would be the ideal way to produce the most accurate earth response (Ghose, 2002). However, variables such as differences in near-field earth materials, changes in source coupling, pad response, machine flexure, and noise all play a role in making estimations of "true" ground force extremely difficult on production surveys.

MASW & Tomography

A single unique data set was acquired along the crest (Figure 23) and another along the toe road (Figure 24) (running parallel to East Canyon Creek) using a towed array. Parameters for these data were selected to allow a subset to be sorted off specifically for MASW and another for turning-ray tomography analysis. Both analysis methods were employed targeting anomalies

Figure removed at request of BoR security personnel.

Figure 23. Towed spread and RAWD. Collecting MASW/tomography data on dam crest. Wood planks were used to protect the dam surface from the hammer blows.

Figure 24. Towed spread and RAWD. Collecting data along the toe road.

within the shallow portion of the geologic sections. The line along the crest targeted both native and construction materials at and in proximity to the rock/concrete contact. The objective of the profile along the toe road was exclusively native rock.

MASW and turning-ray tomography data were acquired using a towed spread of geophones. A contiguous streamer made of reinforced 6-inch fire hose houses thirty 4.5 Hz geophones that are connected to steel shoes attached inside the fire hose (Figure 25). For this configuration, the streamer was dragged behind a skid-steer style loader used to power the mechanically accelerated weight drop (Figure 26). Receiver spacing within the hose assembly was 4 ft and the source was moved 8 ft between adjacent impact points. Continuous surveys were acquired by dragging the spread of geophones behind the source from source point to source point. At each source station the source forward movement was halted, the towing line slackened, and the ground impacted three times. Once all three impacts were recorded, the source was moved forward 8 ft with the firing sequence begun again for the next source station location. With the towed array remaining a fixed distance from the source, all data were recorded with a constant source to closest receiver offset of 16 ft. This offset range was determined to be optimum for the depth of interest, site characteristics, and recorded data properties.

Figure 25. Fire hose and geophone steel shoe. The steel shoe cut through loose surface material and provided a solid ground couple.

Figure 26. Towed spread configuration for data acquired along the toe line.

Borehole

Borehole data including OVSP, ZVSP, checkshot, and frequency/amplitude monitoring were recorded in the crest borehole (Figure 27) and OVSP, ZVSP, and checkshot data were recorded in the toe borehole (Figure 28). ZVSP and checkshot survey data were acquired using two source offsets for all three source configurations (SH, SV, and P). Each source occupied locations 23 ft and 100 ft offset from toe well and 16 ft and 114 ft from the crest well. Frequency/amplitude studies were undertaken with the acentric vibratory source located along the centerline of the dam and near the midway point between the right abutment and uncontrolled spillway (Figure 29). By rotating the vibrator's mass the IVI minivib provided both transverse (Figure 30) and longitudinal (Figure 31) shear-wave data for each downhole receiver location. To ensure the entire recording system was properly polarized with respect to the dam axis (center line), the mass was rotated from a north/south (longitudinal) orientation to an east/west (transverse) orientation at each downhole receiver station. The accelerated weight drop provided compressional-wave energy for all borehole measurements.

Figure removed at request
of BoR security personnel.

Figure 27. Crest borehole (DH-04-1) with downhole geophone cable lying slack on the ground. Cable was slackened after geophone was locked in hole to minimize mechanical noise transmitted through cable.

Figure 28. Cable and alignment rods protruding from the toe borehole.

Figure removed at request
of BoR security personnel.

Figure 29. Bureau of Reclamation researcher removing weight from acentric vibrator bolted to the dam crest.

Figure 30. Vibrator mass/baseplate located on dam crest in transverse configuration.

Figure 31. Vibrator mass/baseplate located on dam crest in longitudinal configuration. Arrows here and in Figure 30 show the axis of the vibrator mass.

Figure removed at request
of BoR security personnel.

Figure 32. Fiberglass rods are used to help align the three borehole tools relative to the vibrator mass and dam axis.

A custom three-pod receiver array, designed and built by the Geological Survey of Canada, was used for all borehole measurements on this project. Each of the three interlocked receiver pods was separated by 6.5 ft (2 m) and capable of independently attaching (locking) to the borehole walls using a surface-actuated mechanical band located on each pod. Three directionally sensitive and uniquely oriented receivers were secured within each pod, each capable of simultaneously and independently recording compressional, in-line shear, and cross-line shear for each shot. This receiver system includes an electronic compass located on the bottom pod allowing surface readout of the system's borehole orientation.

Orienting the receivers when suspended in the borehole was accomplished by physically twisting the entire unit from the surface. To improve the efficiency of this surface alignment activity, fiberglass rods (chimney sweep rods) were attached to the top pod in 4.5 ft (1.5 m) sections (Figure 32). With each pod affixed to adjacent pods by a section of high-speed steel chain, all pods rotated in the hole as a unit. Because high-speed chain only has freedom to move along one axis, the pods could not rotate relative to each other. This cylindrical rigidity allowed mechanical alignment of all receivers to a prescribed orientation while maintaining a fixed pod separation and some relative freedom of movement between pods (this flexibility helped avoid downhole restrictions) while eliminating independent rotation of the pods.

Data were acquired in two boreholes; one located on the dam crest that penetrated both concrete and native rock, a second at the dam toe immediately downstream of the toe fully within native rock throughout the drilled interval. Both boreholes were open (no casing) below the surface casing, thereby exposing borehole tools to native rock complete with several fracture zones. Fractures are considered by many to be the most ominous threat to the unimpaired operation of borehole tools in an open hole, especially for contact tools like calipers and hole-lock geophones. To reduce the threat these features represent to effective operation and retrieval of the three-pod, three-component seismic receiver, operations were limited in areas where fractures were large and represented the greatest risk of tool loss.

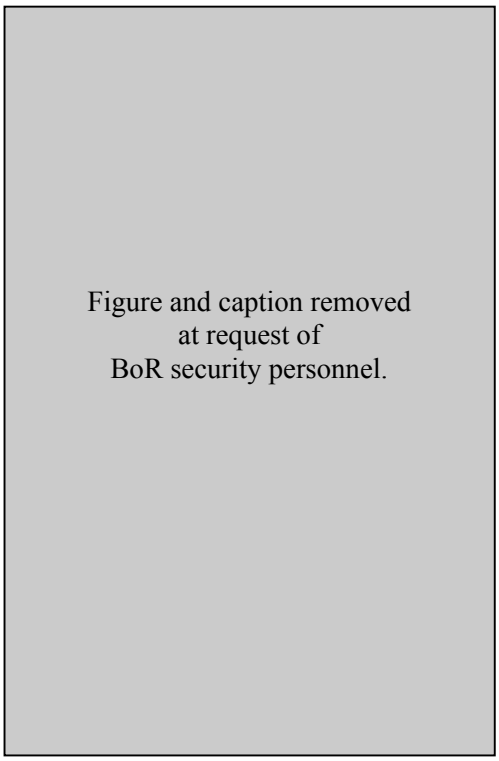

Figure 33.

The crest borehole (DH-04-1) was approximately 50 ft south of the north entrance to the dam crest (Figure 33). Geophysical logs and geologic analysis of samples from this 400 ft deep borehole identified several zones within the borehole where caution would be necessary to avoid getting the hole-lock geophone stuck (Figure 34). To avoid an interval interpreted to contain a large fracture zone, the lowest coupling point by the borehole geophones in the well was approximately 260 ft below ground surface (BGS). Receiver spacing in the borehole was 3.25 ft. Receiver coupling and upward movement of the tool was hindered at several locations above 250 ft BGS in the borehole. One location required significant time and

effort to reestablish upward tool movement. Locations where the tool "hung" correlated with changes in lithology or enlarged fracture zones. Two runs were made in the borehole to obtain measurements from both source-to-borehole offsets.

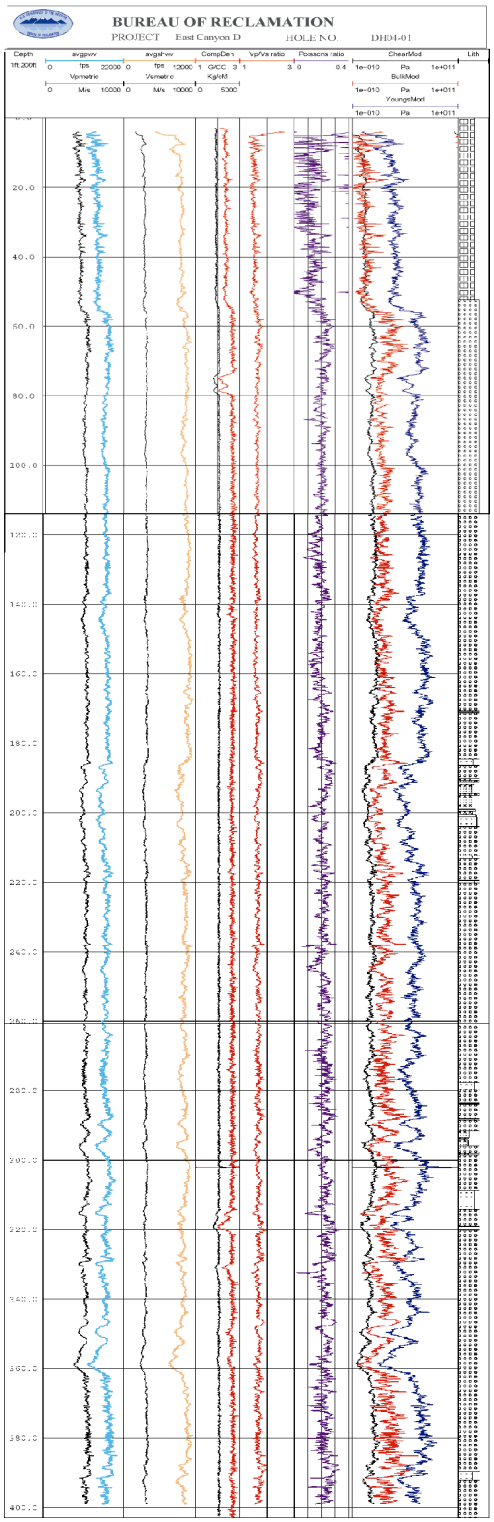

Figure 34. Wireline logs from crest borehole DH 041.

The toe borehole was near the east end of the toe road, approximately 200 ft from the outlet (Figure 35). Considering the dipping nature of the surface rocks, it was not possible from the information available at the time of the borehole survey to correlate features between the two boreholes (Figure 36). Maximum depth measurements made in the toe borehole were about 212 ft BGS. As at the crest, survey measurements were taken every 3.25 ft with the exception of a zone between 153 ft and 185 ft where the tool hung several times, raising concerns about the

Figure 35. Toe borehole with tool being positioned and locked in place.

Figure 36. Abutment road with dipping bedding planes of the massive conglomerate exposed.

possibility of dislodging rocks loosely clinging to the sidewalls and wedging the tool in the hole. This problem is especially daunting considering the vertical nature of the locking bands. Two runs were made in the borehole to obtain measurement from both source-to-borehole offsets.

Data Processing

Data processing for each different component of the wavefield was accomplished using software and techniques appropriate for the method. Seismic reflection data were processed using well-established high-resolution methods. MASW methods were used for analyzing the surface-wave energy, a somewhat more recent but nonetheless reliable processing method. Turning-ray tomography analysis focused on first arrivals picked from data recorded with the towed spread. Tomography and MASW processing at this site used the same data set. VSP data were processed using a very simple approach that targeted unique slope dependencies characteristic of upcoming reflections. Downgoing energy is generally composed predominantly of tube wave, air wave, and direct wave.

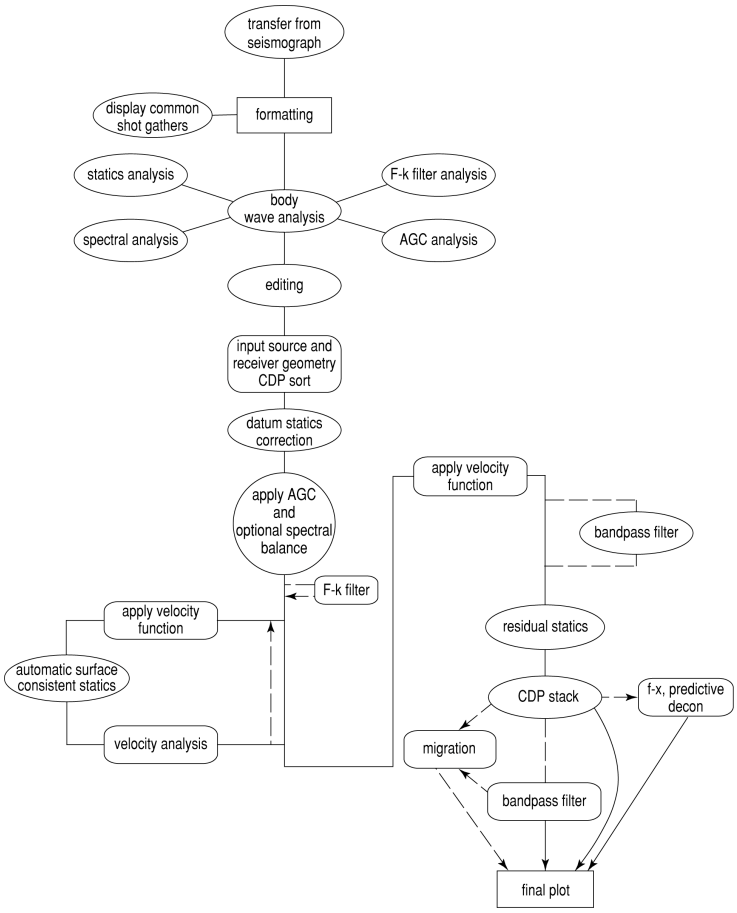

Figure 37. Processing flow for reflection data.

Seismic Reflection

High-resolution seismic reflection data, by its very nature, lends itself to over-processing, inappropriate processing, and minimal involvement processing. Interpretations of high-resolution shallow reflection data must take into consideration not only the geologic information available, but also each step of the processing flow and the presence of reflection events on raw unprocessed data. Processing for the reflection portion of this study included only operations or processes that enhanced signal-to-noise-ratio and/or resolution as determined by evaluation of reflections interpreted directly on shot gathers (Figure 37). For the most part, processing of high-resolution shallow-reflection data is a matter of scaling down conventional processing techniques and methods; however, without extreme attention to details, conventional processing approaches will produce undesirable artifacts. In-field processing of the reflection data ensured the data acquired were of sufficient quality to provide meaningful interpretations and to permit the integration of the different modes when final processing was completed.

The basic architecture and sequence of processing steps followed during the generation of the final stacked sections was similar to conventional petroleum exploration flows (Yilmaz,

1987). The primary exceptions related to the step-by-step QC necessary for the highest confidence interpretations of shallow features and realization of full resolution potential (Miller et al., 1989; Miller et al., 1990; Miller and Steeples, 1991) (Figure 37). Specific distinctions related to the emphasis placed on velocity analysis (Miller, 1992), lack of extensive wavelet processing, care and precision placed on muting, step-by-step analysis of effects of each operation on reflected energy, limiting statics operations to maximum shifts no greater than one-quarter wavelength of the dominant reflection energy with large correlation windows, and coincident iterative velocity and statics analysis.

Brute stacks processed using a somewhat ordinary flow did not possess a signal-to-noise ratio sufficient to interpret. A combination of the high density and diverse orientation of fractures prevalent in outcrop along these survey lines are ideal sources of scattered seismic energy. Combining the fractures with the significant dip in bedding planes observed in outcrop within the massive conglomerate, it is no wonder that an ordinary or routine approach to data processing is not effective. To reduce the affects (especially on NMO velocity corrections) of the dipping layers, only traces recorded from updip receivers (relative to the source) were included in the stacked sections. This approach improves the focusing of the receiver spread and reduces the blurring associated with gathering traces with the same source-to-receiver offset but markedly different reflection-wavelet arrival times due to dip-dependent travel paths along a dipping surface.

Data were processed using WinSeis2 beta (next generation of WinSeis Turbo), a commercial software package available from the Kansas Geological Survey.

Surface Wave

Surface-wave data processing requires extraction of the optimum traces from each shot that provide the smoothest and most interpretable fundamental-mode dispersion curve, which, when inverted, produces the most accurate shear-wave velocity estimate (Figure 38). These optimum trace gathers were processed to velocity cross-sections with SurfSeis (a proprietary software package from the Kansas Geological Survey that facilitates use of MASW for continuous profiling). Each shot gather generates one dispersion curve that was assigned a surface location corresponding to the midpoint of the analyzed spread of receivers. Care was taken to ensure that the spectral properties of the t-x data (shot gathers) were consistent with the maximum and minimum

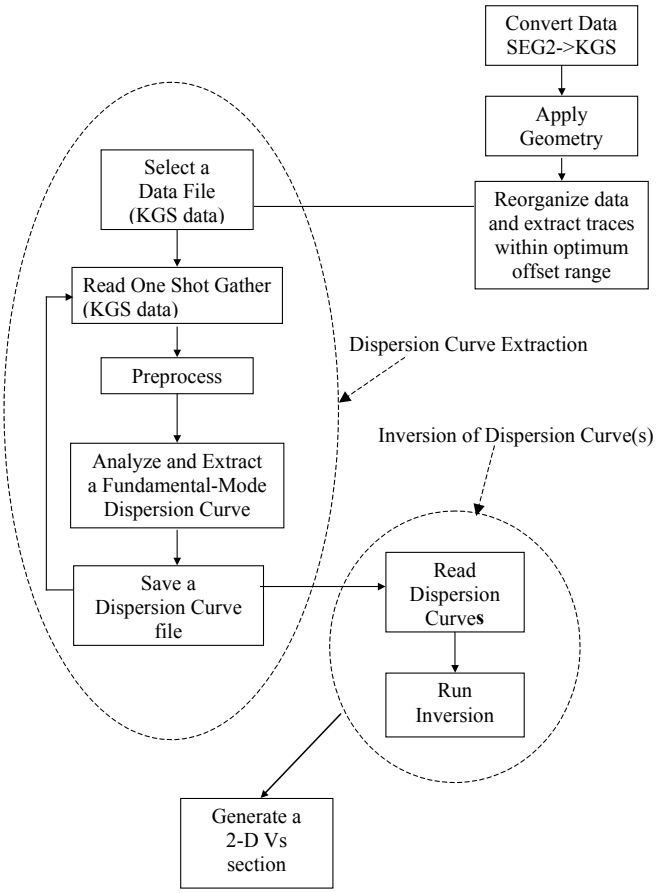

Figure 38. Processing flow for MASW data.

f-v_c values (v_c is the phase velocity of surface waves) contained in the dispersion curve. Shear-wave velocity maps generated along each profile line were optimized for resolution using several approaches including deblurring and slope filtering. Wavefield maps have been generated based on optimized receiver spread offset for depths of interest and data characteristics.

To increase the signal-to-noise ratio and to improve convergence during inversion, a new technique called Filtering of Dispersive Seismic Event (FDSE) was used to suppress higher modes on some shot records (Park et al., 2002). This method removes higher modes through filtering in the frequency domain and avoids the detrimental artifacts that are observed in dispersion analysis if higher modes are removed using time-domain muting. Because SurfSeis was designed to invert fundamental-mode Rayleigh-wave energy only, inclusion of higher-mode or body-wave energy can inhibit convergence.

Turning-ray Refraction Tomography/First Arrivals

Turning-ray tomography is possible when there is a velocity increase with depth. Such an increase would cause the propagating seismic rays to turn back to the surface following Snell's law of refraction. First-arrivals were picked from the MASW towed-spread seismic data. Using the first-arrival trends in the observed first arrivals, an initial model was created using standard refraction solution techniques. The initial model was passed to an inversion program that estimated first arrivals based on that model and then iteratively changed the model until the predicted first arrivals matched (within a minimal error) to the observed first-arrivals on the actual shot records. Several inversion runs were made using the initial model to converge on conditioning parameters appropriate for this data set. Fine-tuning of the initial model is optimized when best-fit conditioning parameters were used during preliminary analyses.

Considering the resolution requirements and redundancy in rays penetrating each subsurface cell within the depth interval of interest, it was necessary for first arrivals to be picked for all traces on every shot gather.

By analyzing the correlations between the model and observed data, the final inversion data was used for quality control of the first-arrival picking routines. In some instances, secondary first-arrival analysis was necessary to converge on a "good" solution. Additional quality control was achieved by verifying that the 2-D Vp/Vs data were reasonable and consistent with other data from this site.

VSP

As is the case with surface-seismic reflection processing, key to the production of an accurate corridor stack from VSP data is identification and time correction for up-traveling reflected signal. Processing of VSP data is relatively straightforward and involves fewer steps than high-resolution seismic-reflection processing (Figure 39).

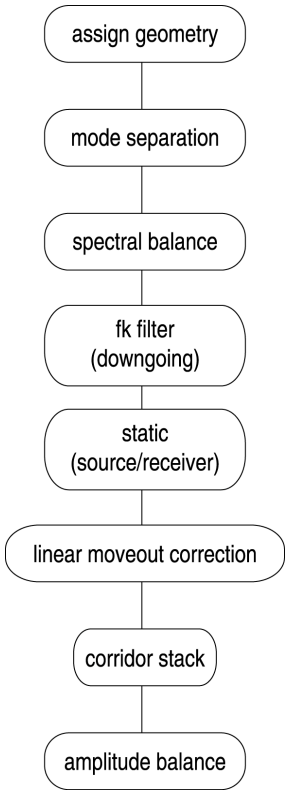

Figure 39. Processing flow for VSP data.

A lack of upcoming energy with a linear velocity, trackable from trace-to-trace on shot gathers, precluded construction of a velocity function suitable for moveout correction. Data were therefore processed to enhance upcoming energy without continuation and production of a corridor stack. Shot-gather data possessed several seismic features characteristic of unique geologic features potentially significant to this study.

QA/QC

The data acquired and processed on this survey were managed to ensure the highest quality and most accurate acoustic representation possible at this geologic setting. State-of-the-art techniques were used in a fashion that was appropriate and verified with step-by-step QA/QC. The most important (possibly even essential) QC information are samples of shot gathers. Raw and processed shot gathers allow geophysicists and geologists to make determinations as to the authenticity of processed seismic sections. Seismic processing software and techniques are very powerful tools that, if not used properly, can and most likely will result in unrealistic interpretations.

The equipment and recorded data were continuously monitored during acquisition to ensure the highest quality sections. Receiver response and sensitivity were monitored using a modified tap test performed after planting each geophone or group of geophones. The continuity and leakage of each active station was meter monitored prior to each shot, with approach, equipment changes, or modifications made to stay within accepted limits. The system was subjected to a series of pre-acquisition tests designed to ensure consistency in system noise, and precision in digitally stored data. Visual monitoring of overall signal-to-noise ratio, environmental noise, DC bias, and variations in the optimum recording window was continuous throughout the survey. Preliminary in-field processing provided excellent insights into data quality and need for real-time parameter adjustments. Velocity information key to optimizing the reflection surveys was obtained from borehole data (Figure 40).

Figure 40. Mobile processing facility on-site and used to perform data quality checks. Three on-board computers and two plotters with Ethernet connections to the seismograph allow rapid in-field data analysis.

Discussion and Interpretation

Unfortunately, none of the seismic methods worked up to their full potential at this site. This can be related, to a large part, to the extremely difficult geology and abundant noise present on this site. The dipping conglomerate with extremely high density and diverse orientation of local fractures in association with the steep cliff face along which the seismic reflection data were acquired provided excellent scatter and out-of-the-plane reflection sources. As well, abundant noise was present at this site. The most detrimental sources of noise included the wind, water moving through the outlet works, and vehicles (cars, boats, trucks).

Even with these daunting seismic obstacles, reflections appear to have been recorded and when processed with dip-specific directional data, it was possible to provide insights into the subsurface geology at this site. Estimates of average velocity as a function of depth from bore-hole data was possible. These data allow zones with potential velocity anisotropy to be proposed and variation in seismic properties of the rock to be suggested. Surface-wave and tomographic studies provided some unique information about the lateral variability in velocities within the shallowest portion of conglomerate.

Discussion of the various data sets from this point will be divided into the toe area and crest area. Data recorded in these two different settings can be related in a very general sense, but lack strong correlation due to differences in near-surface material and rock properties resulting from the extreme dip observed in bedding within the conglomerate and physical separation of boreholes.

Toe Data

MASW

The same towed-array data were used for both MASW and tomography analysis. Shot gathers recorded with the towed array suffered from coupling inconsistency, a characteristic observed on most towed-array data acquired in rough terrain (Figure 41). Significant intra-spread variability in receiver coupling is not surprising considering the rocky, uneven toe-road

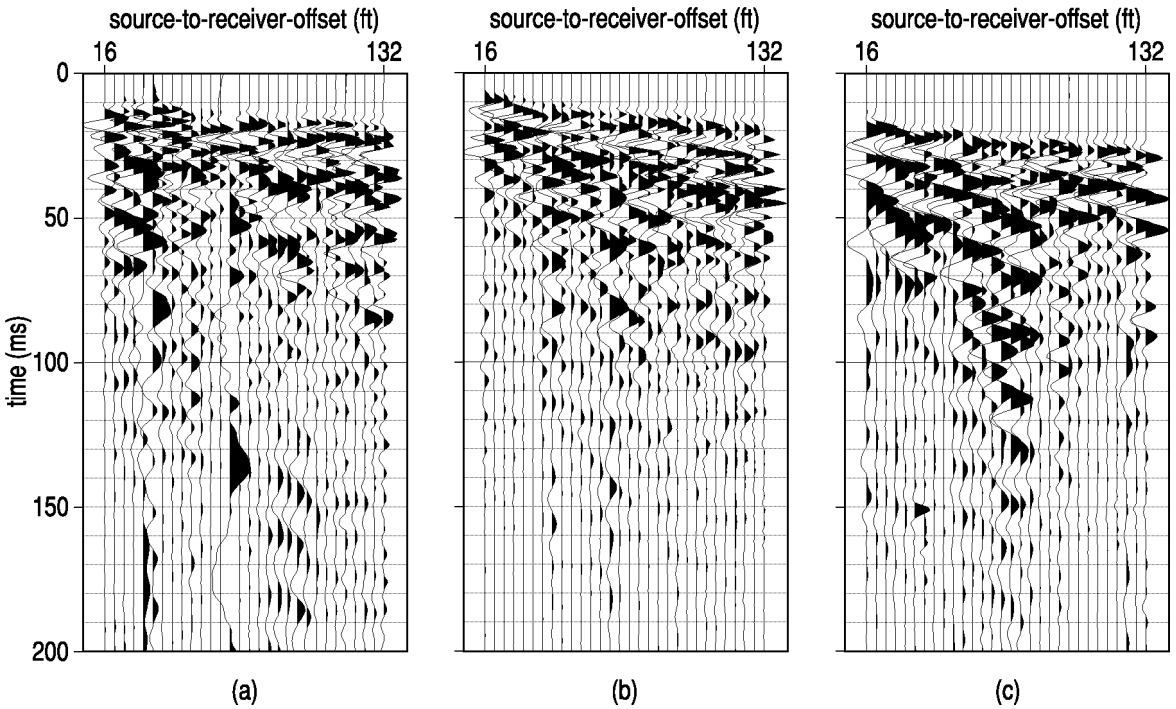

Figure 41. Shot gathers from along the toe line using the towed spread and RAWD. Extreme lateral inconsistency in seismic energy makes slope analysis (of the type used for MASW) very difficult. First arrivals appear to surface from static delays and wavelet inconsistency. Most of these problems are likely related to coupling with the rocky, gravelly road surface.

surface (Figure 42). Some of the apparent trace-to-trace differences in wavelet and arrival times are related to geology. Abnormalities related to geology and not coupling issues can be easily separated on common-receiver gathers. However, the most detrimental data degradation is easily distinguishable on shot gathers and removed during the data-editing component of the processing flow. Some of the differences in trace-to-trace wavelet and spectral properties make use of the data beyond first-arrival analysis precarious.

Figure 42. Towed spread along the toe road. The steel shoe on the bottom of the fire hose acts to slice through the loose material to improve receiver coupling. Cobbles and larger gravel would cause the shoe to ride up and degrade the overall coupling.

On towed-spread shot gathers surface-wave energy is very difficult to uniquely separate from noise and body-wave energy (Figure 41). Beyond the first few shot stations and last few shot stations on the toe line, surface-wave energy lacked sufficient coherency to confidently interpret either spectrally in the fk domain or from phase velocity/ amplitude relations in the time domain. This lateral variability limited the use of MASW to only the extremes of the line. Considering subsequent tomography analysis and near-surface velocity structure, it is not surprising surface-wave energy would not propagate along this line for distances sufficient to calculate dispersion curves in the middle of the line.

By using only data with interpretable Rayleigh waves on shot gathers, MASW analysis was restricted to just a few shots on each end of the survey line, thereby inhibiting contiguous estimates of Vp/Vs away from the borehole in the shallower portion of the geologic section. Fortunately, dispersion curves from these few shot gathers did allow estimates of shear velocity near the borehole and therefore permit comparisons to be made with direct borehole measurements and tomography estimates.

Dispersion curves for these first three shot gathers change dramatically one to the next (Figure 43). More than eighty percent of the receiver stations used to produce any three sequential shot gathers are the same along this line. With such a high percentage overlap in recording stations it is reasonable to expect a great deal of similarity in both the time-domain shot gather and the frequency/phase-velocity dispersion curve. The dramatic differences observed in the first several shot gathers in both domains along this profile are indicative of the high degree of variability present in both rock properties and receiver coupling.

Several shot gathers from the west end of the profile have interpretable Rayleigh-wave arrivals that are sufficiently coherent to produce defensible dispersion curves (Figure 44). With the increased thickness of unconsolidated fill material over the conglomerate bedrock near the curve in the road at the west end of the profile, surface waves have become a distinguishable component of the wavefield. As well, with this near-surface velocity structure and fill/bedrock layer geometry another familiar coherent noise event has become evident, higher-mode surface

waves. Higher modes are evident on the dispersion curve plots as higher frequency events with similar geometry and phase velocities as fundamental-mode energy.

The Vs section for the small segments at the beginning and end of the survey line is consistent with borehole data and reasonable for this site (Figure 45). Since lower-velocity fill material thicker than a few tenths of a foot is only present on the ends of the toe-road survey line it makes sense that dispersive Rayleigh waves are only observed at the ends of the profiles. Based on the MASW data a zone approximately 80 to 100 ft wide of low-velocity unconsolidated or semi-consolidated materials is present from just east of the borehole to about 70 or 80 ft west of the borehole. This low-velocity zone is at least 60 ft thick, very localized, and defined on the west by an abrupt increase in velocity. Considering what we know about surface-wave dispersion phenomena, the layer represented by the low-velocity gravel fill over the bedrock is not thick enough for dispersive surface waves to propagate and bedrock is laterally disturbed to a point that coherent surface waves cannot propagate.

Borehole and MASW data match reasonably well considering the minimal number of dispersion curves available for analysis. Borehole Vs ranges from 4000 ft/sec at around 30 ft BGS to about 6200 ft/sec at 120 ft or so BGS. In comparison the Vs structure at the well location based on MASW ranges from 3000 ft/sec at 30 ft BGS to 6500 ft/sec at 120 ft BGS. This is an outstanding match considering the very low signal-to-noise ratio of the surface-wave energy.

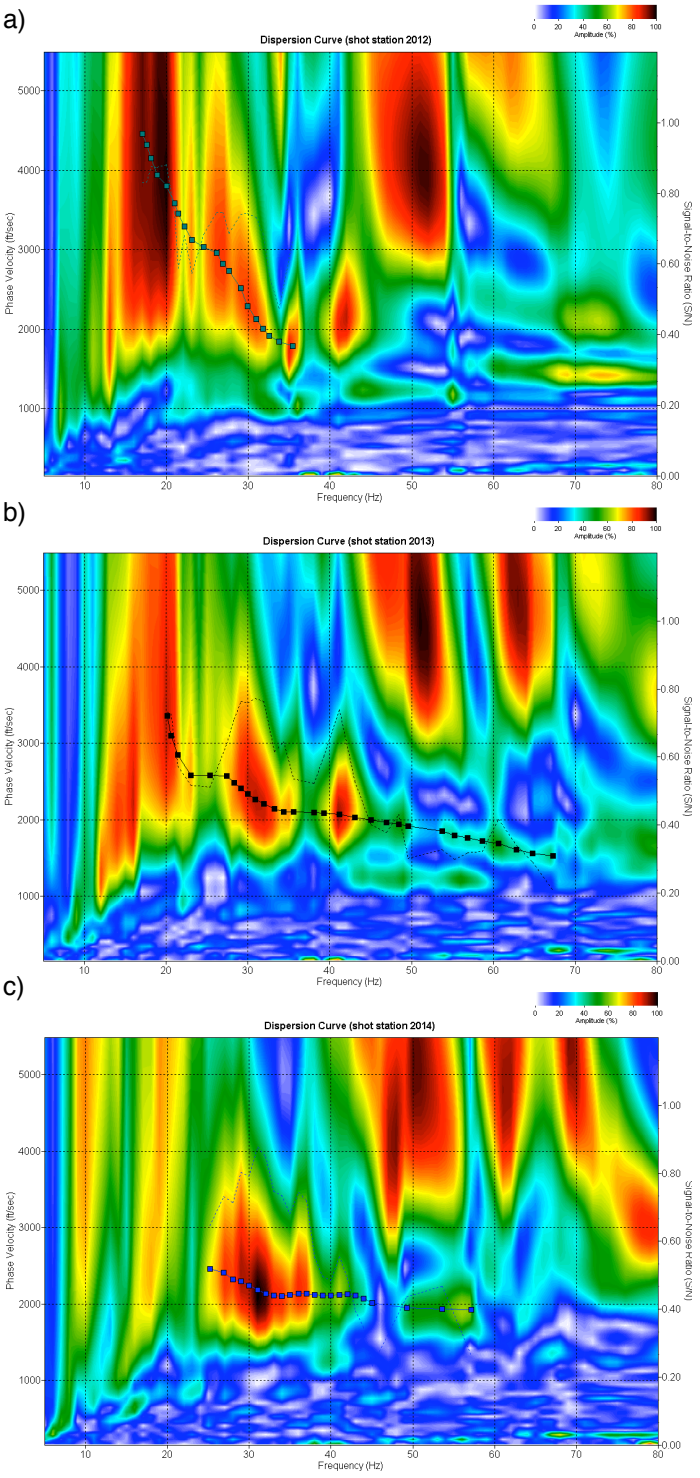

Figure 43. Dispersion curves of the first three shot gathers on east end of profile from towed spread. Eighty percent of the data used to produce these dispersion curves are from the same receiver stations. Changes in receiver coupling and material properties are dramatic and lend to this variability.

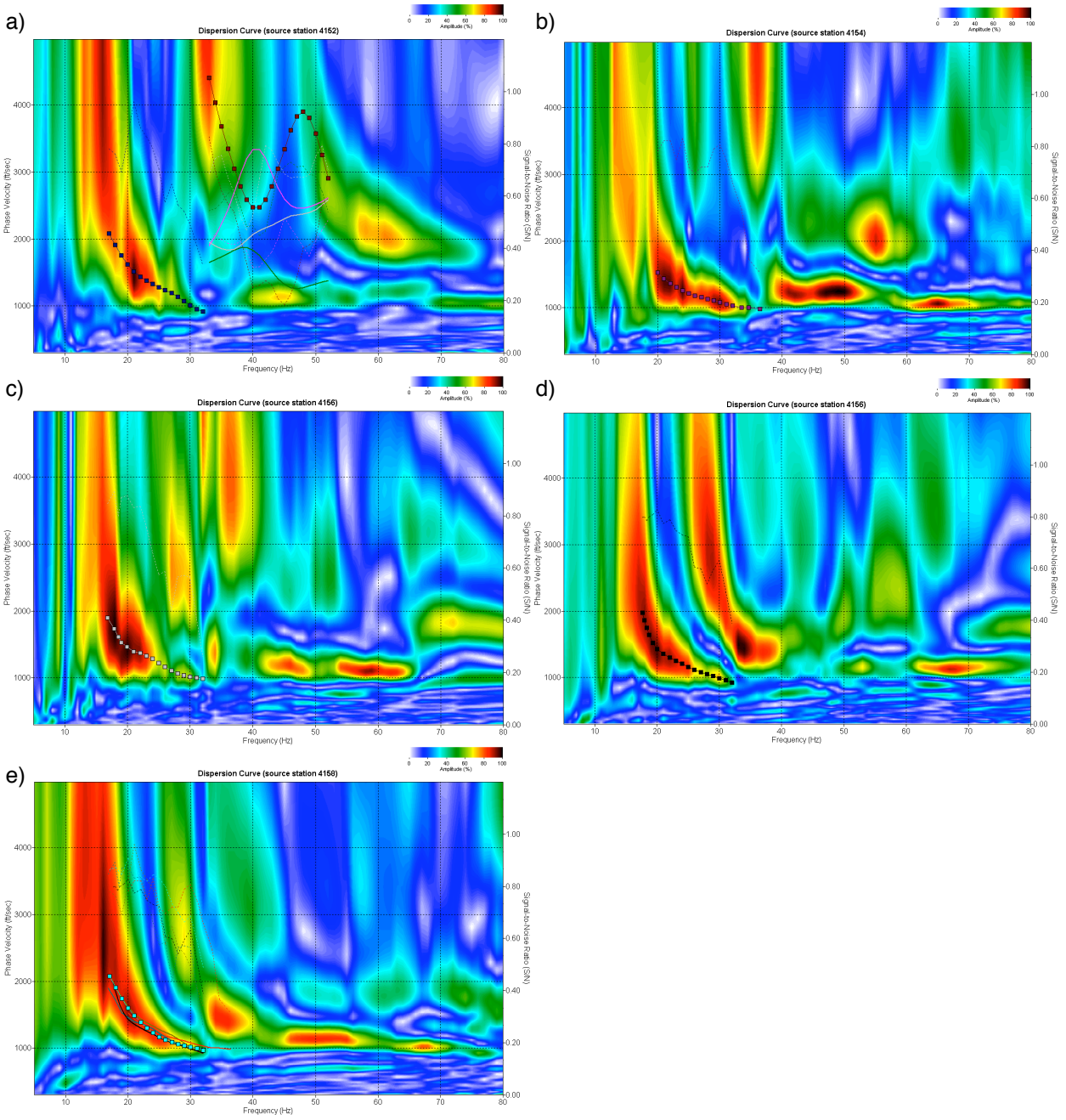

Figure 44. Dispersion curves from the west end of the profile possess significantly more consistency in comparison to the eastern end of the profile, and dramatically more than the middle of the line. High modes begin to become more pronounced as the thickness of the lower velocity unconsolidated fill increases.

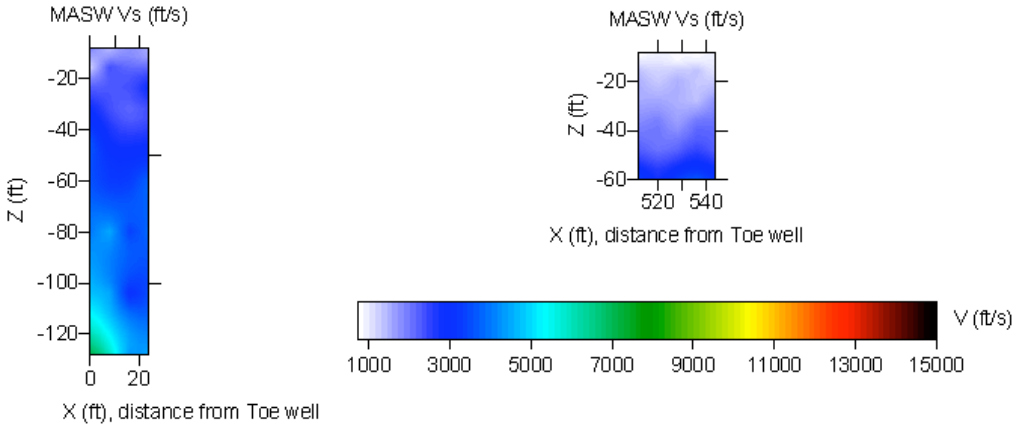

Figure 45. Shear-wave velocity cross-section estimated from inversion of Rayleigh-wave dispersion curves using MASW techniques along the toe road profile.

Turning-Ray (TR) Tomography

First-arrival wavelets recorded using the towed spread lacked a high level of trace-to-trace consistency (Figure 41). This variability made picking the instant in relative time representing the earliest onset of energy at each receiver station a challenge. TR tomographic analysis as used here is the only effective way to map the extreme topography of the high-velocity bedrock relative to the thin, low-velocity fill material. Granted, none of the basic refraction assumptions have been violated, but considering the laterally discontinuous nature of the conglomerate (dipping beds with unconsolidated materials within near-surface bedding planes, fracture zones filled with compacted rubble) significant lateral variability in compressional-wave velocity would likely have been incorrectly inferred from localized changes in bedding geometry and conglomerate features.

Two-dimensional turning-ray tomography software specially developed at KGS to map dipping surfaces was used to invert first-arrival selections made on tow-spread data. First arrivals could be picked with reasonable confidence on about two-thirds of the shot gathers recorded along the toe line. Noise from the dam outlet saturated a majority of traces on the east end of the profile. In general, the velocity range as observed on the tomography cross section for the upper 20 ft is reasonable in comparison to that measured at the well. Granted, the closest Vp value estimated from turning-ray tomography data is about 80 ft from the well and the material around the well possesses very different shear velocity from that 80 ft further west. A Vp range of around 6000 ft/sec at about 30 ft BGS to 10,000 ft/sec at 120 ft BGS observed on borehole check shot data is consistent with the trend extrapolated from the MASW data and observed velocities on the tomography data.

An extremely high bedrock velocity clearly dominates the velocity structure as defined by tomographic analysis of the towed-spread data (Figure 46). Interesting to note is the pinnacle-looking topography of the bedrock surface. These geometries are consistent with more resistant zones within layers of this steeply dipping conglomerate unit representing highs and fractures or more erosionally susceptible bedding planes manifested as bedrock lows. Also interesting to note is the correlation between the tomography and MASW data sets between 500 and 550 ft offset from the well. Both data sets suggest a bedrock valley between 40 and 60 ft deep near

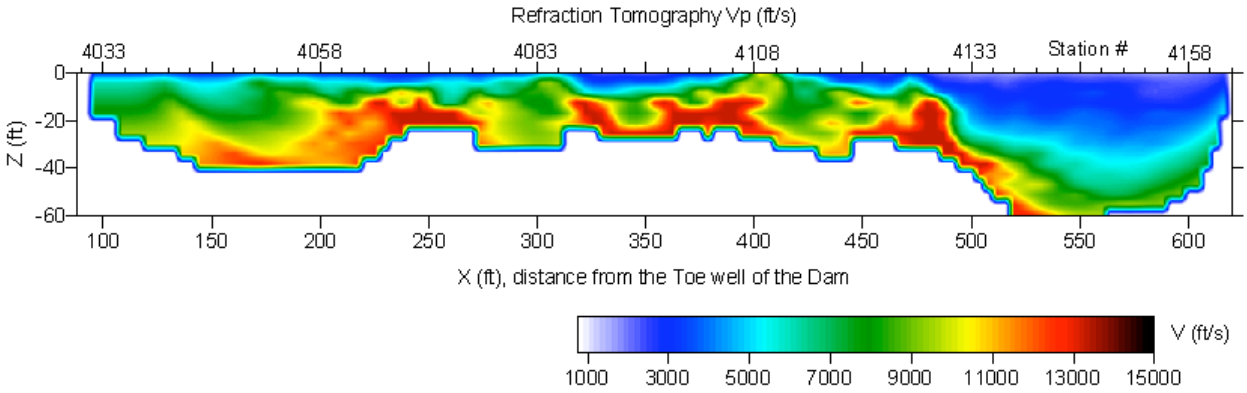

Figure 46. Refraction tomography along the toe-road profile using first arrivals from traces recorded using the land streamer (towed spread).

540 ft offset from the well. At this far west end of these two profiles the Vp/Vs appears to be around 2.5 at 20 ft BGS which is quite reasonable for compacted, unconsolidated sediments. Near the surface (~5 ft) the Vp/Vs is likely closer to 3-4 based on qualitative comparisons of these two profiles.

Through the mid-portion of this profile the compressional-wave velocities exceed 12,000 ft/sec at depths less than 20 ft. Of particular interest are the low velocity zones at 300 ft and 425 ft west of the toe well nestled between high-velocity units. These lower-velocity zones are likely fractures or bedding irregularities that are more readily eroded and therefore lower velocity. It is feasible to suggest that these low-velocity areas related to less resistive zones identified in outcrop (Figure 47). Looking from the dam crest onto the toe road these less resistive beds within the massive conglomerate can be easily identified as they plunge to the west beneath the toe road.

Figure 47. (right) View of the toe road from the dam crest. Dipping layers can be defined by changes in material "weatherability."

Reflection

Both compressional- and shear-wave reflection data were recorded along the toe line. Neither compressional- nor shear-wave recorded data were optimum, due to the short line length dictated by physical limitations of this site. Also, the dip of bedding planes observed in outcrop within this massive conglomerate and cliff face immediately south of the toe line reduced signal-to-noise and limited processing to only up-dip traces (that is, for each shot gather only receivers that were up-dip of the source). Considering the stacking velocity in this case will likely be significantly different from true average velocity, borehole measured average velocities were used for time-to-depth estimations.

Compressional

The compressional-wave reflection section for the toe line is characterized by spotty coherency and abundant scattered energy (Figure 48). Two areas appear to have coherent reflection arrivals consistent with reflections interpreted on shot gathers. One group of events is above 100 ms and lies beneath stations 2000 and 2030. Between station 2020 and 2030 there appears to be an increased number of diffractions or scatter events likely indicative of faulting or fractures. With the limited-to-indistinguishable offset in the interpreted events across this diffraction/scatter zone, it is likely this is a fracture zone much like those observed in outcrop on the south canyon wall immediately downstream of the dam (Figure 49).

Because of the condensed spread geometry both the offset and fold distribution is inconsistent across this profile and has resulted in a wedge of subsurface coverage. However, it is still possible, even with this very limited amount of data, to extract meaningful information about the subsurface beneath the toe line. Looking at the major coherent events on this profile, three trends are prevalent (Figure 48). First, two events at approximate depths of 300 ft and 600 ft appear to dip to the west between the east end of the line and about station 2040. It is possible but unlikely that the 600 ft event is a multiple. Considering the borehole TD'd at around 250 ft and did not penetrate the basal contact of the massive conglomerate, it is reasonable to suggest this 300 ft event represent the contact between the conglomerate and underlying shale. Without other collaborative information it is also possible that the 300 ft event is related to a strong contrast, indicative of a material change within the conglomerate and the 600 ft event is the top of the underlying shale.

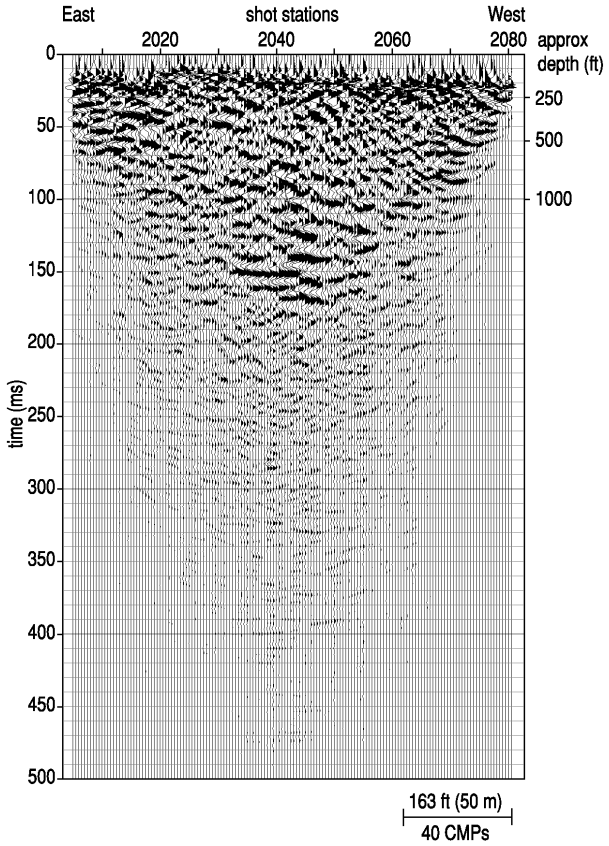

Figure 48. (left) Compressional-wave CMP-stacked section along the toe line. Apparent discontinuous reflection events are influenced by acquisition geometry, proximity of cliff face, fracture prevalent across site, and very unsorted nature of the matrix of this massive conglomerate. Approximate depth scale based on downhole survey in toe well.

Figure 49. View looking south from toe road. Fractures can be interpreted with dips ranging from vertical to horizontal and most angles in between.

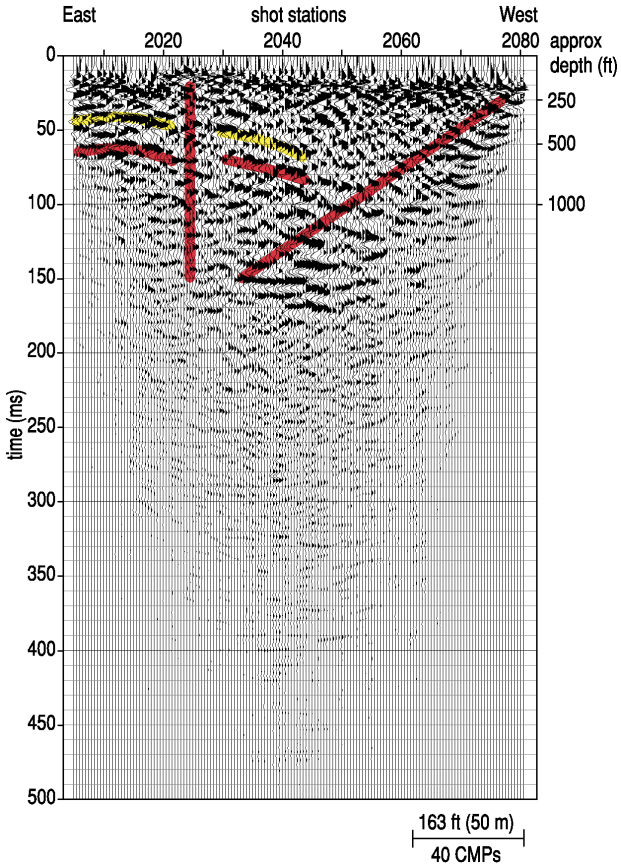

Figure 50. Interpreted compressional-wave CMP-stacked section along the toe line.

A second major unique trend is represented beneath station 2025 and trends near vertical with a very high-angle dip to the east (Figure 50). This feature does not appear to offset the events previously identified at 300 ft and 600 ft to any significant degree. Correlating this feature with the tomography data a pronounced low-velocity zone within the bedrock is apparent at approximately station 4035 ([Figure 46] which matches station 2025 of the reflection data). Considering the resolution and signal-to-noise of these two data sets, this is an outstanding commonality between these two data sets which are targeting distinctly different parts of the near surface.

Finally, a third trend, interpreted based on character, possesses a relatively high-angle dip to the east beginning near the western extreme of this profile (Figure 50). Data characteristics used to interpret this trend were more consistent with a fault plane or high-angle erosional contact than a bedding surface or contact between different lithologies. The dramatic difference in character of events interpreted across this boundary suggests that this trend might represent the contact between the massive conglomerate and the underlying shales at the western extreme of this profile. This trend lacks much in terms of coherent events but can be readily distinguished from seismic property changes. Adding to the support that this is an east-dipping contact is the up-dip specific nature of these data and any contrast with an east dip would not be imaged well if at all.

All things considered, one possible interpretation of these data would suggest the 300 ft event beneath the eastern quarter of the profile is the basal contact of the conglomerate. This contact dips to the west across this fracture zone beneath station 2030 to about station 2060, where at a depth of around 600 ft it abruptly changes dip orientation and begins to rapidly shallow to the west. These observations are quite speculative considering the overall data quality of this compressional-wave CMP-stacked section.

Shear

With the lower-amplitude signal recorded during the shear-wave acquisition it was necessary to apply an automatic gain control and there by increase the migration artifacts observed in the “no data” window below 150 ms on the ends of the line tapered to about 300 ms down to the bottom of the section near the center of the profile (Figure 51). Several coherent events can be interpreted across this section. None of the coherent events appear continuous across the section. Using the shear-wave velocity function measured from the downhole survey in the toe borehole,

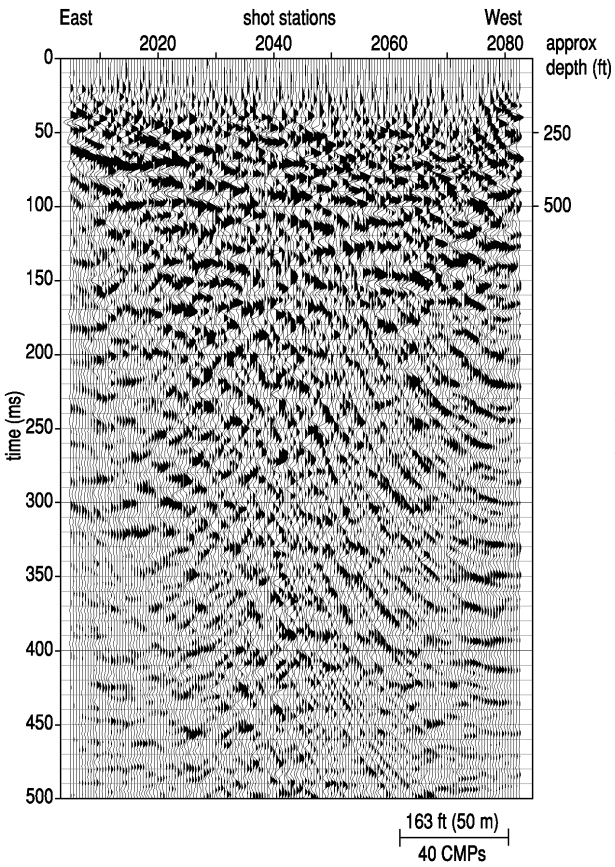

Figure 51. Shear-wave CMP-stacked section along the toe line.

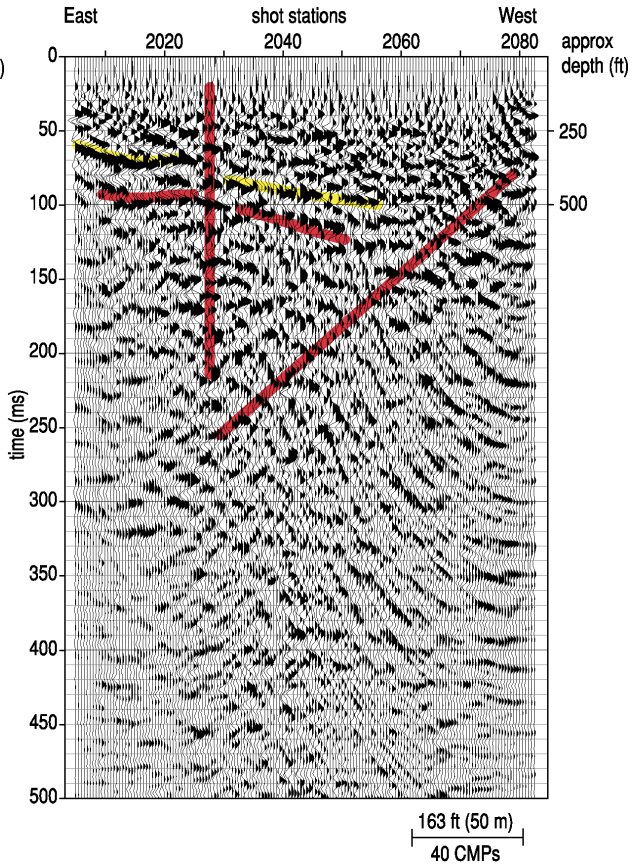

Figure 52. Interpreted shear-wave CMP-stacked section along the toe line.

the average velocity for the shear-wave data is about half that of the compressional-wave data along this profile. On shear-wave data, as with the compressional-wave data, representative average velocities could not be extracted from stacking velocity as defined by curve fitting of the CMP data. Therefore, borehole measurements were used to estimate the conversion from time to depth on CMP stacked sections.

As on the compressional-wave section, several coherent events appear to possess amplitudes just sufficient to emerge from the noise and are interpretable over significant portions of the CMP stacked section (Figure 51). Interpreting this section is complicated by migration artifacts evident as cyclic curved events that appear to originate from the edges of the section. These artifacts result from the incomplete migration that is characteristic of single velocity fk-style migration. However, fk migration is reasonably effective in adjusting dipping reflections with a particular velocity range to more accurately represent the subsurface reflector geometries, and for that reason migration is a necessary evil. Clearly the coherent events on the east end of the profile at 70 ms, 100 ms, and possibly at 150 ms are interpretable at least a third of the way across the profile. These events correlate quite well with those interpreted on the compressional-wave sections.

Using the compressional-wave data as a guide, but focusing on what are truly the highest confidence, interpretable events on shear-wave data, three different dominant trends can be

interpreted on these data (Figure 52). Two events, one at approximately 300 ft and the other at around 500 ft, are clearly traceable from the east end of the profile to around station 2030 where their slopes are altered and character changes slightly. One marked difference between the compressional and shear reflection-looking events on this easternmost part of the section is their geometry. While the compressional-wave events form a very subtle anticline-looking structure, the shear-wave data form a bowl or synclinal-looking geometry. Clearly these both cannot be correct. Considering the high density of artifacts introduced by the migration on the shear-wave data, it is possible without much imagination to suggest the upward curve at the eastern extreme of these events are an induced affect from low fold and migration. This would suggest the anticlinal shape is more representative of the events in this area.

It appears reasonable to interpret the two coherent reflection-looking events across the chaotic zone beneath station 2030 and most of the way across the middle portion of the record (Figure 52). Using the borehole measured velocity there appears to be a reasonable match between the compressional and shear CMP-stacked sections with the maximum depth of the shallowest coherent event (assumed to be the basal contact of the conglomerate) around 500 ft BGS. On the compressional-wave section the depth as estimated at around 600 ft. With everything considered it is likely the true depth to this event is within that range (500 ft to 600 ft).

Again two unique trends mark changes in event character, trace extremely steep-dip angles, and are not direct reflection (Figure 52). The easternmost zone is defined by its chaotic appearance and near vertical geometry. This zone ties reasonably well with the compressional-wave reflection data and with the turning-ray tomography data. Farther west a second trend dipping to the east at a much gentler angle likely marks the western extreme of the conglomerate. Based on the seismic character, this could well be an erosional truncation or a structural feature marking the termination of the massive conglomerate body. The depth and orientation of both these trends match with the compressional and tomography data.

Borehole

Data were acquired in the toe borehole on two separate runs, one with the source around 25 ft from the borehole and a second with the source about 100 ft from the borehole. Close-offset data were used to estimate average velocity and studied for reflection arrivals (ZVSP). Longer-offset data were used only for efforts to identify and enhance reflections (OVSP). At a depth of around 185 ft a series of fractures was encountered that temporarily stuck the tool in the hole. Once the tool was free it was moved to about 153 ft to ensure the tool was clear of this fracture zone. Data collected from the close offset has a gap for this depth interval and the tool was only lowered to 146 ft to make certain that zone was avoided.

Downhole

At this site measurements of average velocity were made using close-offset data with the receiver in the borehole and source on the surface (e.g., downhole). First-arrival measurements were made on compressional-wave data assuming a minimum phase wavelet. This is a reasonable assumption considering the impulsive nature of the source. Shear-wave data first-arrival picks were made under the notion that the wavelet was a Klauder wavelet and therefore zero phase.

Since each shot was recorded on three receivers any shot static was easily identified and corrected. An expectation of this recording equipment was a readily measurable interval velocity. With the three-pod receiver design difference between the three pods for a given shot should represent pure interval velocity with no source static. For these data, the wall coupling or diversity of travel paths due to the dipping and fractured rocks inhibited the uniformity in the source wavelet necessary for the level of precision required to estimate interval velocities.

Close-offset gathers have one unique arrival characteristic. Due to the intentional skip of more than 30 ft of borehole an apparent disproportionate shift in first-arrival times can be observed near the deeper receiver stations (Figure 53). Shear-wave data also have a shift in the time scale so that negative time is displayed. This display format is a result of the correlation method used.

Some trace-to-trace variability in first-arrival wavelets is evident. The exact source of this lack in consistency is not obvious. Since this is an open hole and within a conglomerate rock body, the most likely explanation is receiver coupling and rock variability. It is unlikely, considering the acquisition equipment and approach, that this difference is related to source, start timing, or receiver placement.

Since shear-wave data were produced using the vibroseis technique, changes in band-width of the recorded data will affect the number and amplitude of side lobes on the first arrival wavelet. Therefore, some of the apparent differences observed trace-to-trace could be related to changes in the transmitted/recorded energy spectrum.

Average velocity for the three receiver orientations was overall consistent, but a few borehole receiver stations appeared locally erratic (Figure 54). Compressional-wave average velocities in the shallower part of the borehole (<50 ft) were between 6000 ft/sec and 7000 ft/sec. In several places significant changes in velocity over a single receiver interval or two can also be tied to changes in the wavelet. From 50 ft BGS downward to about 150 ft BGS the average compressional-wave velocity increased steadily from about 6500 ft/sec to over 12,000 ft/sec. During that same interval the shear-wave velocity ranges from 5500 ft/sec to around 7000 ft/sec. Comparing the compressional and shear velocities through that interval the Vp/Vs remains relatively consistent at around 1.5 (±0.2). This Vp/Vs is rather low in comparison to most sedimentary rocks; however, this Vp/Vs ratio is consistent with the borehole sonic data.

Shear-wave data were acquired with two different polarized source and receiver orientations. Data from longitudinal and transverse source/receiver orientations relative to the axis of the dam provide a glimpse at anisotropy within this fractured, high-velocity rock formation. Clearly between about 90 ft BGS and 140 ft BGS the transverse (E/W) shear energy consistently appears 10% to 15% faster than the longitudinal (N/S). Beyond about 200 ft BGS the average velocity of the two shear-wave orientations appears to align with little or no directional dependence of velocity.

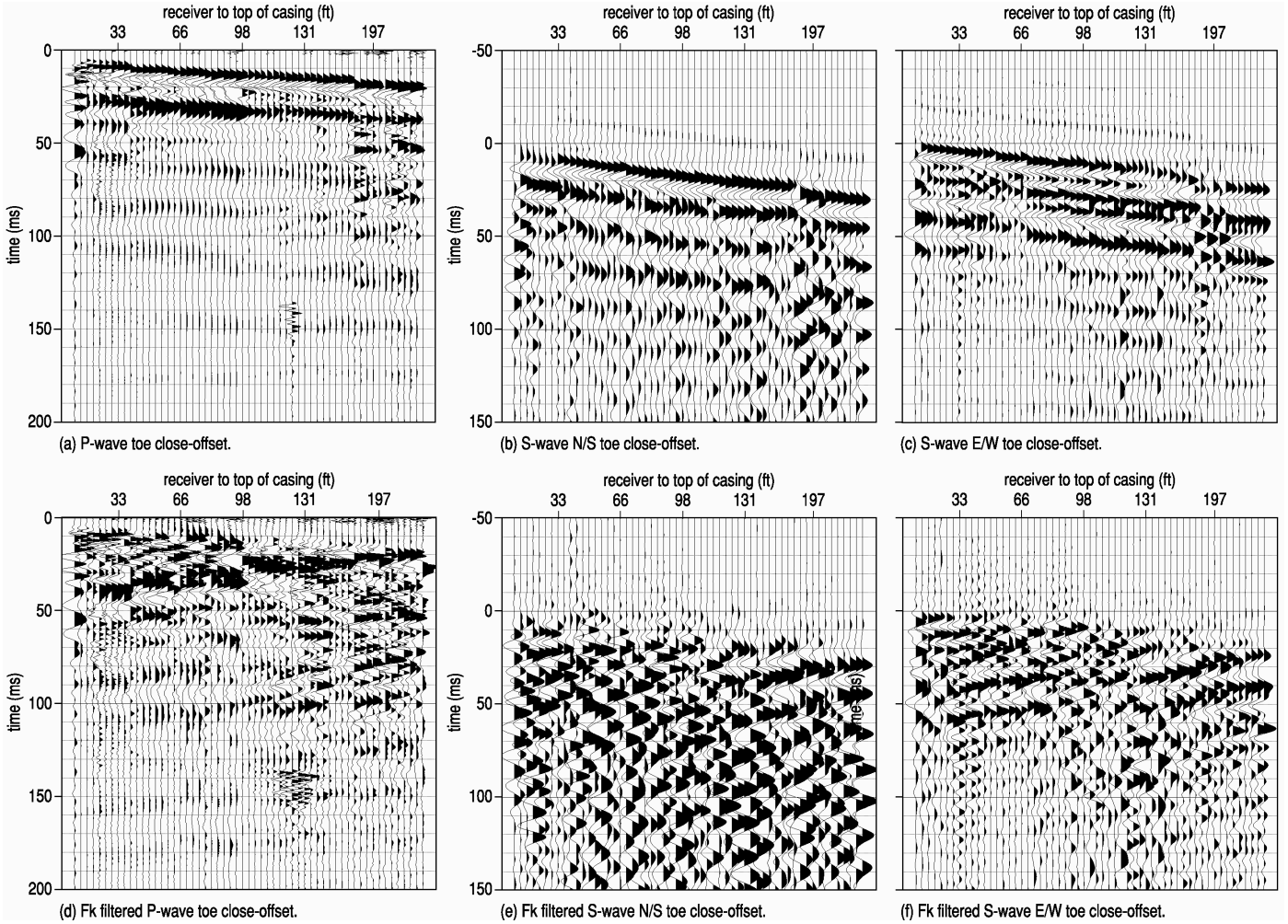

Figure 53. Downhole seismic data, close offsets, toe borehole, from compressional (a), transverse shear (b), and longitudinal shear (c), fk-filtered wavetrains of compressional (d), transverse shear (e), and longitudinal shear (f).

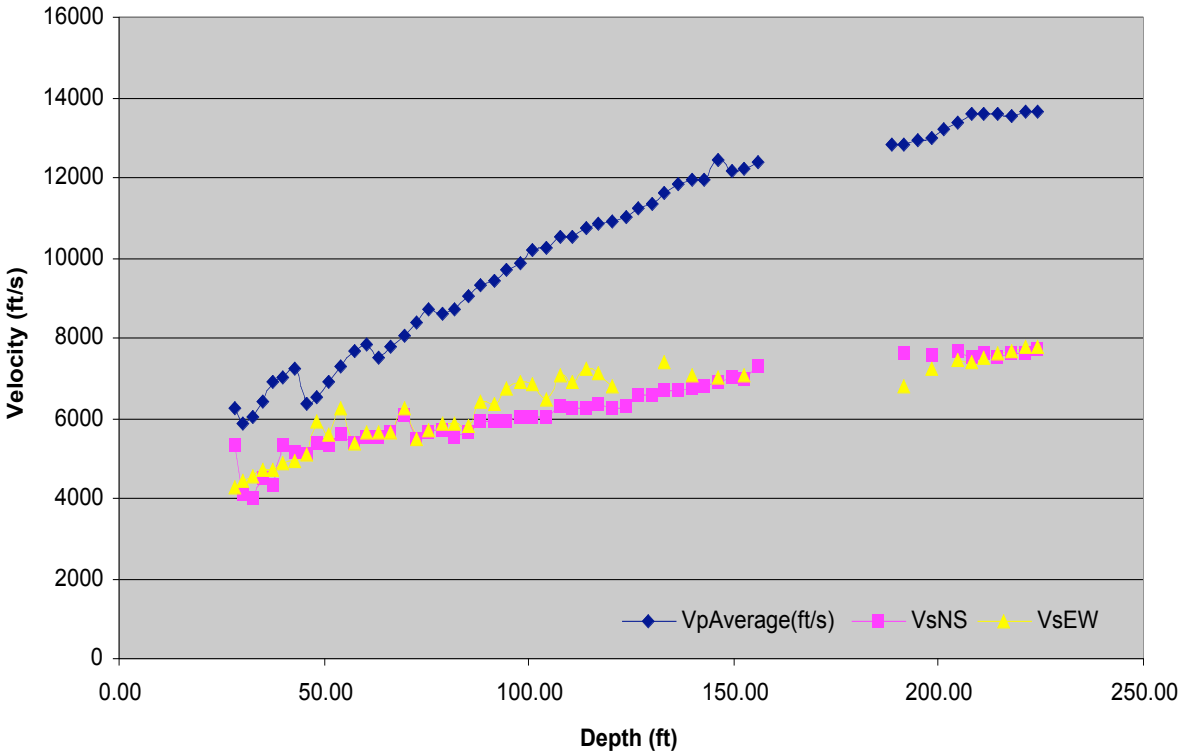

Figure 54. Average velocity calculations based on first arrivals measured when sources were at the close offset (7 m).

VSP

VSP data from this site were not moved out to compensate for receiver depths and then corridor stacked. These two steps in normal VSP processing were not undertaken due to a lack of confidence that the coherent linear events observable on shot station gathers after fk filtering are reflections.

The primary distinction made in the discussion of downhole versus VSP is in the analysis of first-arrival times versus the full recorded wavefield. Looking at both close- (Figure 53) and long-offset (Figure 55) data, several important observations can be made. First, downgoing energy dominates the records. Second, wavetrain differences observed between groups of traces is quite pronounced, suggesting geologic or borehole variability. Third, there are pronounced differences in the frequency and arrival geometry between longitudinal and transverse shear-wave energy. Fourth, source-offset differences change the arrival characteristics of the wave-field. Fifth, the scatter characteristic of fractures in the borehole walls is evident at around 200 ft BGS in shear-wave data, especially longitudinal polarized data.

Reflections on VSP data appear as linear events dipping downward in the direction of the shallower stations. The reflection events intersect the first arrival of the trace recorded at the depth the reflector intersects the borehole. Therefore, any reflected energy will have a slope opposite relative to downgoing energy. Since direct wave and tube wave are both downgoing energy, a slope filter can be designed to remove all downgoing energy, resulting in a section with

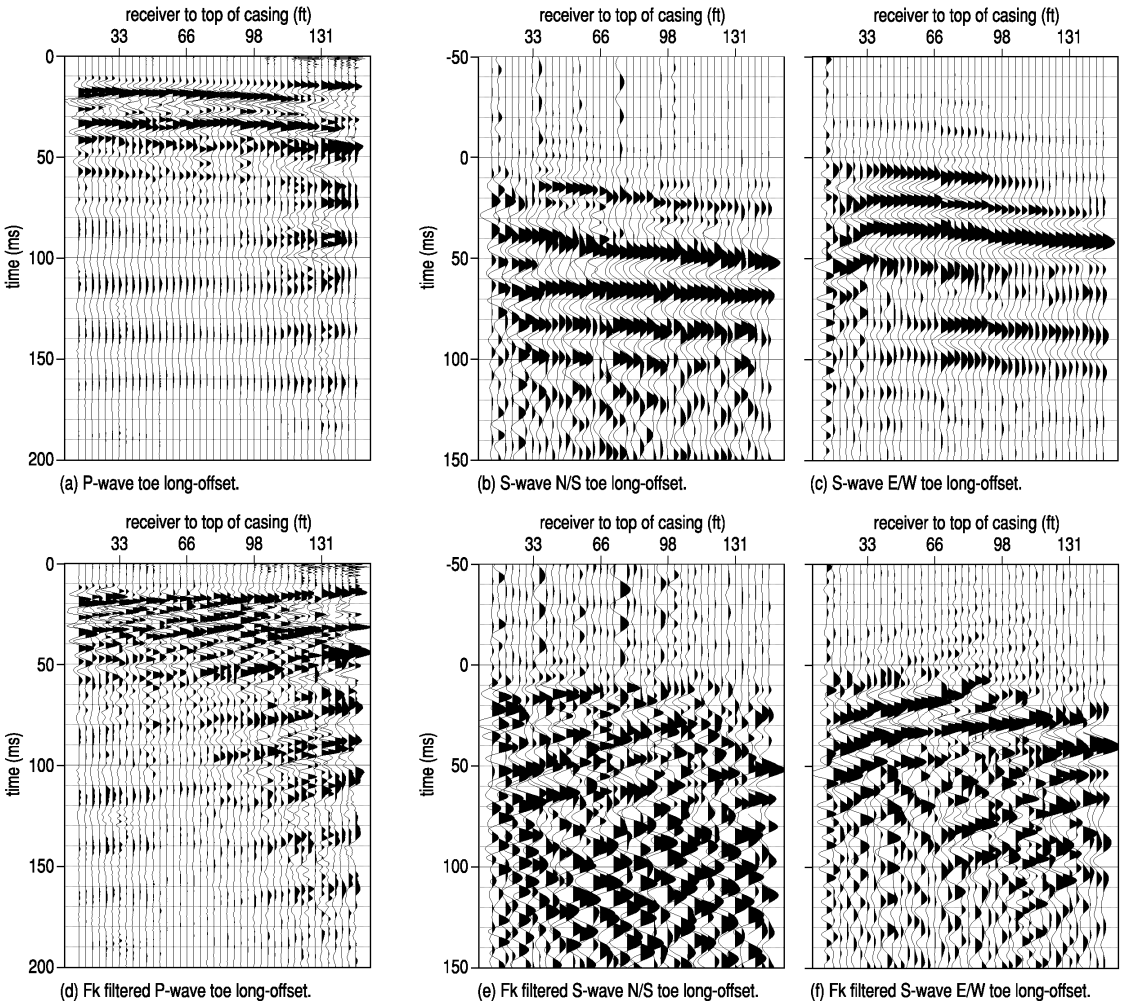

Figure 55. Downhole seismic data, toe borehole, long offsets, from compressional (a), transverse shear (b), and longitudinal shear (c), fk-filtered wavetrains of compressional (d), transverse shear (e), and longitudinal shear (f).

only reflected, diffracted energy, and/or aliased noise. Data after such a slope or fk filter has been applied have a dominant reverse slope component, much of which is a processing artifact.

Compressional-wave VSP data appear to have several interpretable linear events with reverse dip after fk filtering (Figures 53 and 55). On both data sets (close and long offset) these reverse-dip events are most pronounced on traces from deeper borehole locations. Two events interpretable on both sections should probably be considered primary. These events are from about 25 ms and 30 ms (one-way travel time) after depth correction. These two events when converted to two-way travel time are consistent with the reflections interpreted on CMP stacked sections. It is also clear that reflections and scatter arriving from out of the plane are quite pronounced on these data.

Shear-wave VSP data quality is strongly influenced by the orientation of the source and receivers (Figures 53 and 55). VSP gathers of N/S and E/W oriented data all have intra-gather consistency but lack uniformity in arrival patterns or waveforms between the different orientations and offsets. These differences are clearly related to the geology. If the differences were related to coupling, tool, or source, there would not be the clear consistency within like-parameter gathers. Processsed (fk filtered) and raw gathers from E/W oriented parameters possess the strongest evidence for reflections on shear data. E/W data also are of higher frequency and signal-to-noise ratio.

Processed N/S VSP gathers have unique dominant wave patterns that are likely related to fractures and the orientation of those fractures. Energy arriving in the first few cycles past the first arrival appear to lack coherency in the upcoming wave propagation (negative dip) when all downgoing energy is filtered off. Study of the unprocessed sections reveals what appears to be scatter patterns on deeper receiver stations, primarily from around 98 ft BGS and 205 ft BGS. This distinctive difference in recorded wavelet and scatter-controlled arrival pattern suggests these rocks do have a strongly polarized nature with regard to impingent shear-wave energy. Therefore, rock response to seismic energy will not likely be azimuthally uniform.

Crest Data

Data recorded on the dam and along the right abutment are all categorized as crest data for purposes of this report. Data include a compressional- and shear-reflection line along the right abutment; a towed-spread profile along the top of the crest; 3-pod, 3-component recording in the borehole; and fixed 3-pod, 3-component recording above, at, and below the concrete/rock contact.

MASW

Data acquired along the dam crest as part of the MASW and tomography study used the towed spread and vertical impact source (RAWD). This component of the study was to our knowledge the first time MASW has been attempted fully along the crest of a concrete dam. With the extreme vertical dimension of this dam it is reasonable to assume no energy was reflected back to the surface from the upstream and downstream faces of the dam, therefore, surface-wave energy is traveling fully within the half-space. The dispersive nature of the surface wave should be severely impacted by the uniform velocity of the dam. Dispersive surface-wave energy was observed, raising even more questions concerning the type of surface-wave energy actually recorded.

Analysis of the surface-wave data was undertaken under the premise that surface-wave energy was dominated by the fundamental mode of the Rayleigh wave. For a high-velocity earth model without significant changes in velocity (i.e., layering) the surface wave will not be dispersive (velocity changing as a function of frequency) and therefore a realistic dispersion curve cannot be measured and shear-wave velocity model cannot be estimated. These data were dispersive, indicating that weathering affects vertical and horizontal stress changes within the dam, which may give rise to vertical velocity changes (Figure 56).

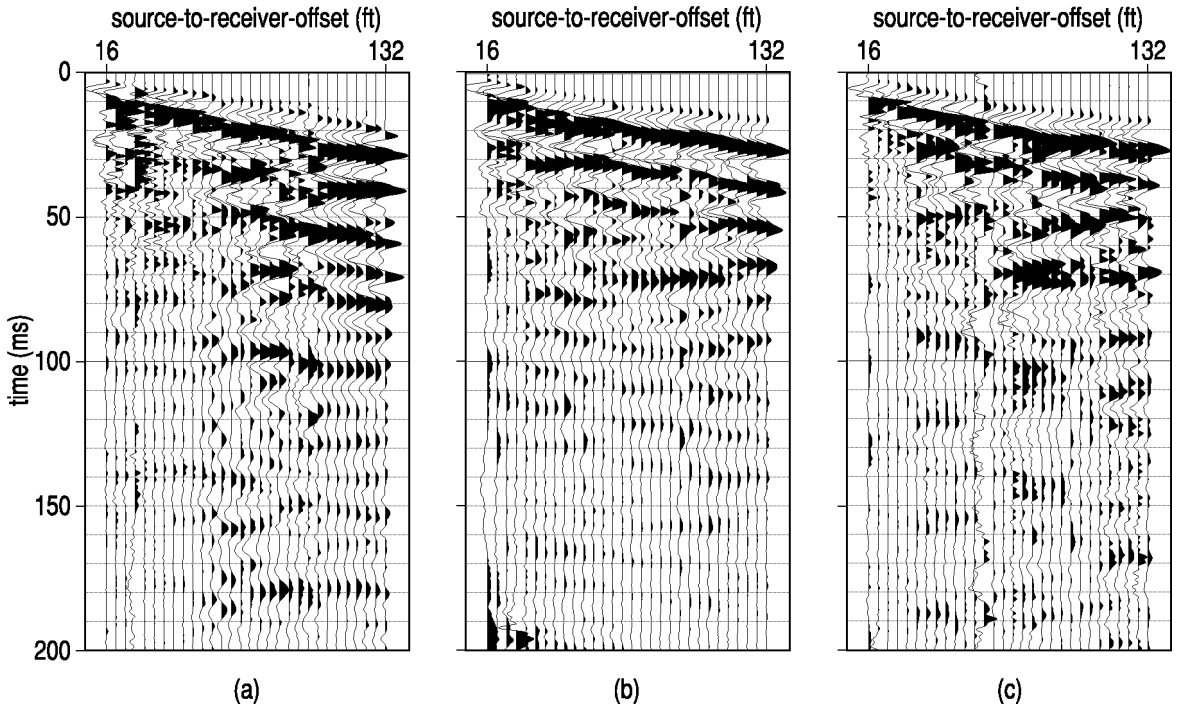

Figure 56. Shot gathers from on the dam using the towed spread and RAWD. Consistency in first arrivals is much improved on the dam in comparison to the toe. Considering the dimensions of this concrete structure, it is not surprising the dispersive character of the surface wave is difficult to distinguish, because of the insignificant vertical shear-modulus variation.

Dispersion curves from across the dam demonstrate both the difficulty in interpreting surface-wave dispersion curves from these data and the apparent inconsistency in dispersion-curve characteristics and properties (frequency/velocity relationship) (Figure 57). Considering the consistency in the concrete surface of the dam and the uniformity of receiver and source coupling to that surface, data (shot gathers, dispersion curves, and velocity profiles) were expected to be extremely consistent across the crest line. After a casual scan of the dispersion curves it is clear the frequency/velocity relationship changes across the dam and more than anticipated with depth. Also, the thrust block on the right side may be influencing data from the right side because rock is shallower under the thrust block. Clearly questions that must be asked and cannot be answered with these data alone are "Is all this energy fundamental surface wave?" and "What is the correct interpretation of these curves?"

Inverting these dispersion curves to estimate shear velocity provides a glimpse of the internal properties of the dam (Figure 58). Using laboratory measured shear- and compressional-wave velocities as general guides in analyzing these data, interesting observations can be made. First, with a laboratory-measured shear velocity of around 7000 ft/sec (Carmichael, 1989) most of the upper 50 ft is consistent with expectations within what we will call experimental error (~10%). Below about 60 ft the velocity rapidly increases to 10,000 ft/sec, which is approaching laboratory measured compressional-wave velocities. However, these laboratory measurements were not made under the kinds of stresses experienced by this dam structure, and probably not with the larger aggregate sizes typical in concrete dams. With the high-velocity nature of concrete and the overall size and stiffness of the concrete dam it was clearly difficult to excite

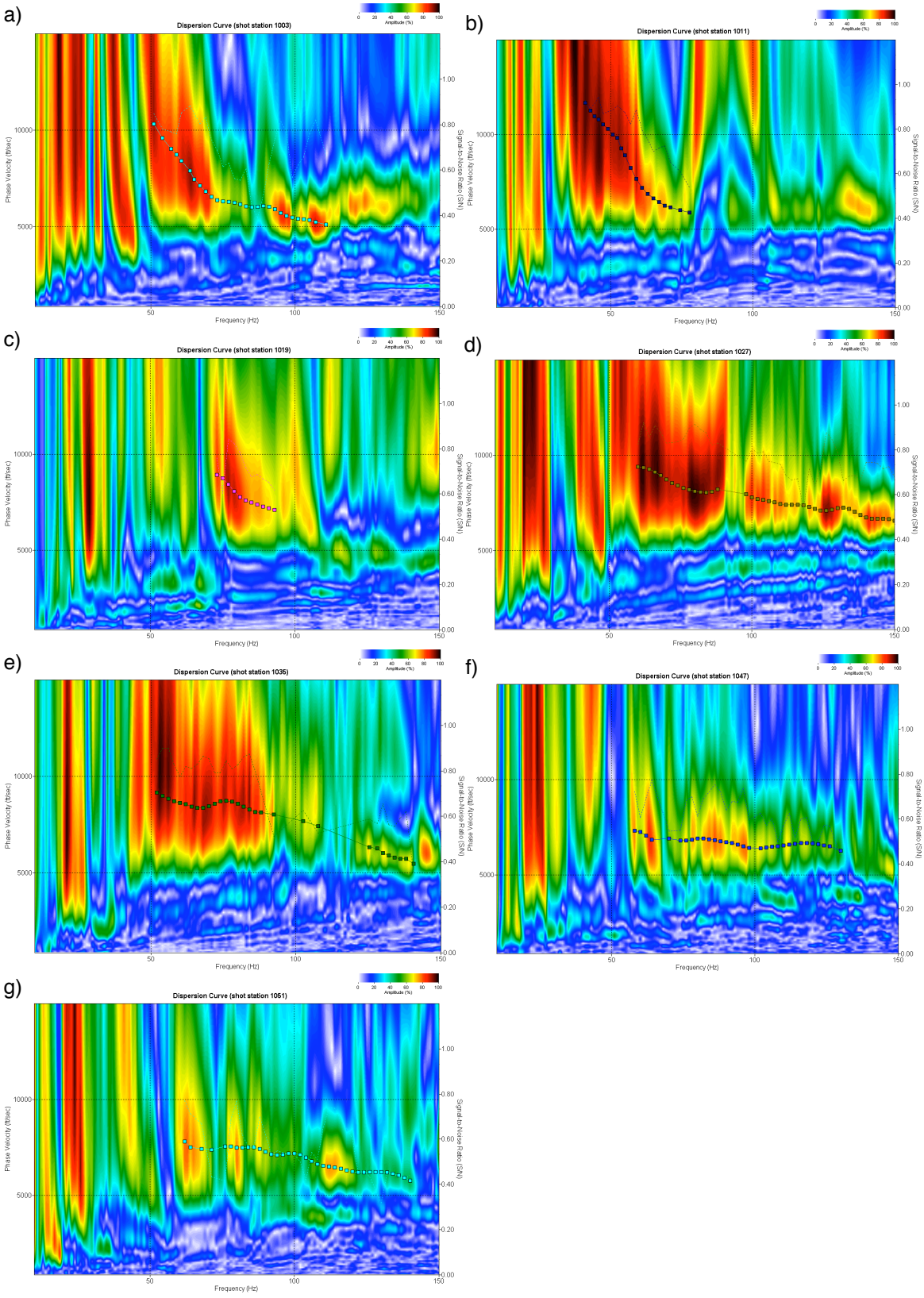

Figure 57. Dispersion curve images from MASW data from the top of the dam.

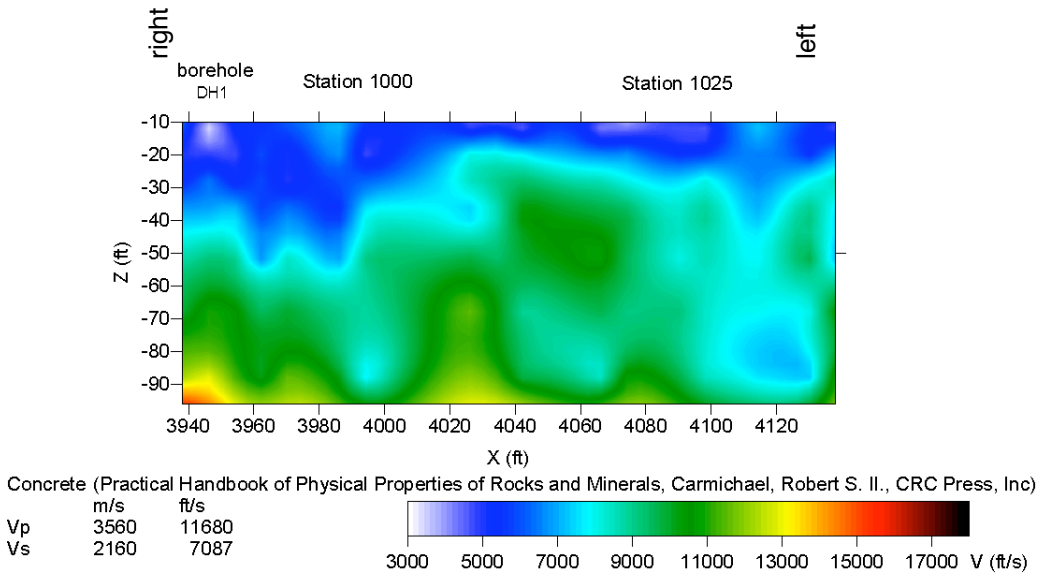

Figure 58. Vs cross section using MASW method on data acquired along the crest road using the towed spread and RAWD.

lower-frequency surface waves in the dam. This lack of lower-frequency energy has depth-limited the use of MASW and as with any technique, as the limits of investigation are approached, error increases.

General analysis of the MASW Vs-velocity cross-section highlights an interesting consistent characteristic of these data (Figure 58), which might have some structural significance. Focusing on the gross trends in the cross section, subtle irregularities can be observed that might be related to changes in seismic properties within the dam. Most notable is the relative increase in velocity in the shallower part of the section beneath station 1015 (4040 ft) and the relative decrease deeper in the section beneath station 1030 (4120 ft). These kinds of changes in velocity could be related to material characteristics of the dam or possibly geometric dependencies of surface-wave propagation within the very curved, thin concrete dam. For consideration: shear-wave velocity will increase with elevated stress once the linearity of stress/strain relationship as defined by Young's Modulus is exceeded at very high stress.

Turning-Ray Tomography

Tomography analysis was undertaken on the same data set used for the MASW investigation of the dam structure. Unique to tomography analysis is the exclusive use of first arrivals only. Therefore the source wavelet was minimum phase and the arrival time was consistent with the first onset of energy. With the extremely high velocity and relatively short source to receiver offset range most of the energy returning to receivers as first arrivals within this 120 ft spread were from the upper 10 ft to at most 15 ft (Figure 59). The compressional-wave cross-section possesses a bowl like appearance that is only happenstance consistent with the geometry of the entire dam structure (Figure 59).

Excluding low ray coverage on the ends of the profiles, the image area extends from around station 1000 (4000 ft) to 1045 (4180 ft) with velocities ranging from about 7500 ft/sec to

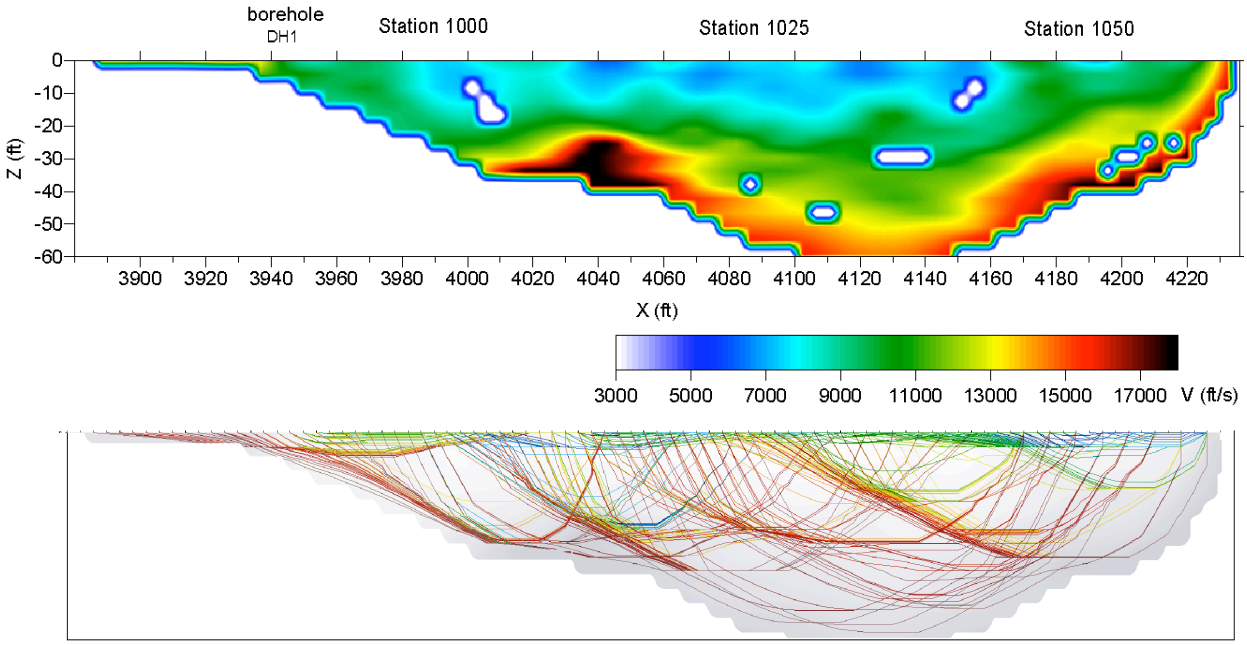

Figure 59. Vp cross section using turning-ray tomography analysis on minimum-phase first arrivals from data acquired using the towed spread and RAWD. White areas indicate lack of ray coverage.

over 12,000 ft/sec in the upper 20 ft (Figure 59). This lower than expected compressional-wave velocity in the upper 20 ft (based on laboratory measurements) could be related to several things including less competent concrete near the surface, low-velocity material dominating the lift line between each pour of concrete, or geometric effects of this curved structure. If this velocity structure accurately represents the dam, this clearly indicates a zone with an extremely low Vp/Vs ratio, possibly suggestive of substantial strength. However, without deeper ray penetration it is difficult to establish trends or to understand what the data represent.

Reflection

Reflection data along the right abutment were plagued by several problems, which inhibited the overall quality of the data. Noise was a primary problem and included natural noise sources (wind, scatter of seismic from fractures and valley walls, water moving downstream) and cultural noise (outlet works passing significant volumes of water, active acentric vibrator testing on dam, vehicle traffic [boats, cars, and bikes]). Since all data were acquired on the road with receivers in the road ditches, trace-to-trace consistency suffered from a lack of uniformity in the receiver coupling and even with the asphalt surface the subgrade changed significantly at different source stations impacting the consistency within CMP gathers. Adding to the difficulty was the crooked line recording necessary to optimize receiver and source coupling in this rough terrain.

<u>Compressional</u>

Compressional-wave data from along the abutment is characterized by guided waves, surface waves, refractions, and scattered body and surface waves with little in the way of symmetry about the source station or clearly distinguishable reflection arrivals (Figure 60). A possible reflection event is interpretable at about 200 ms in the updip direction relative to the

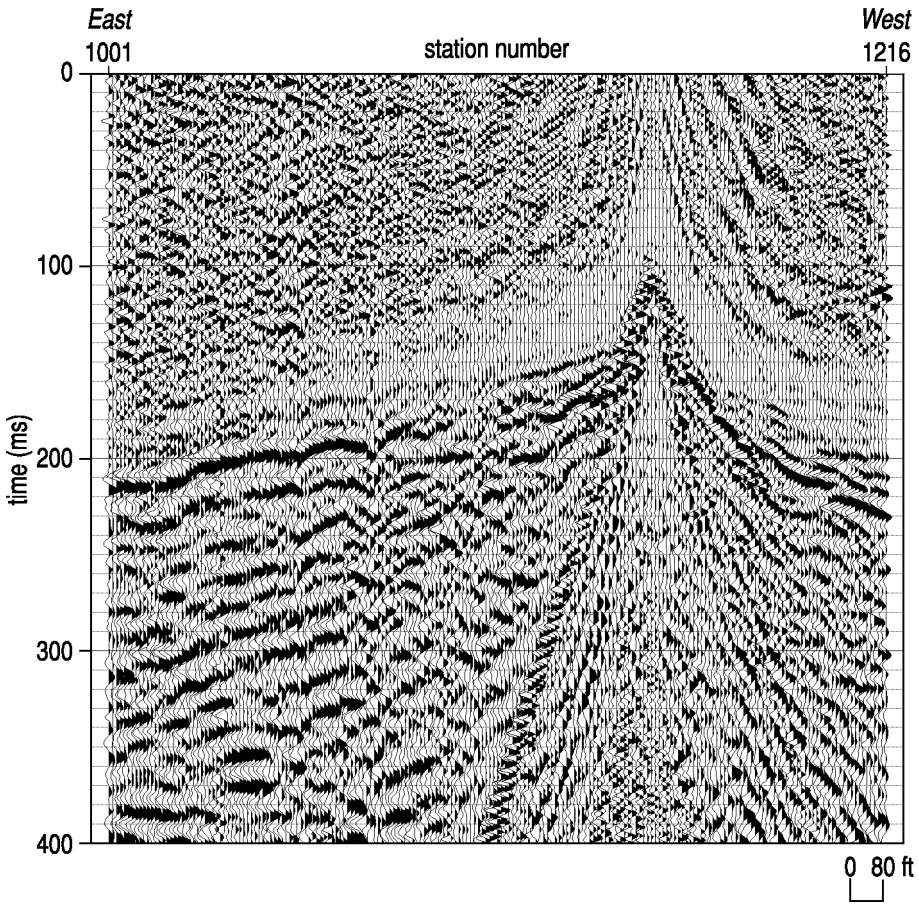

Figure 60. Shot gather using vibrator as source about two-thirds of the way downstream of the dam overlook. A subtle yet notable event that has reflection characteristics can be observed at around 200 ms. This record has a 100 ms delay due to the correlation parameters chosen.

source and geology. Another candidate reflection is evident at about 150 ms. These reflections are from approximately midway across the line, therefore will match most closely with reflections on stacked section around station 1060 to 1080. Broken and geometrically disturbed semi-coherent arrivals within what should be considered the "optimum reflection window" are characteristic of most shot gathers across this profile.

CMP-stacked compressional-wave data have a somewhat "wormy" appearance as a direct result of the many surfaces representing contrasts (reflectors, scatterers) and their wide range of angles relative to the spread geometry (Figure 61). Without a strong reflecting event observed on VSP data it is difficult to determine the exact static shift necessary to align the reflections with reflectors. However, since these are correlated vibroseis records the source wavelet is zero phase and zero time is consistent with the maximum amplitude of the wavelet. These CMP data have been static shifted to align as closely as possible with real time zero. A portion of the shallowest wavelet is clearly truncated by time zero and in actuality extends into negative time, something that is quite possible for extremely shallow reflections. However, for our case to be on the safe side the first full wavelet is assumed to be direct or refracted energy and is therefore not interpreted as anything but coherent noise.

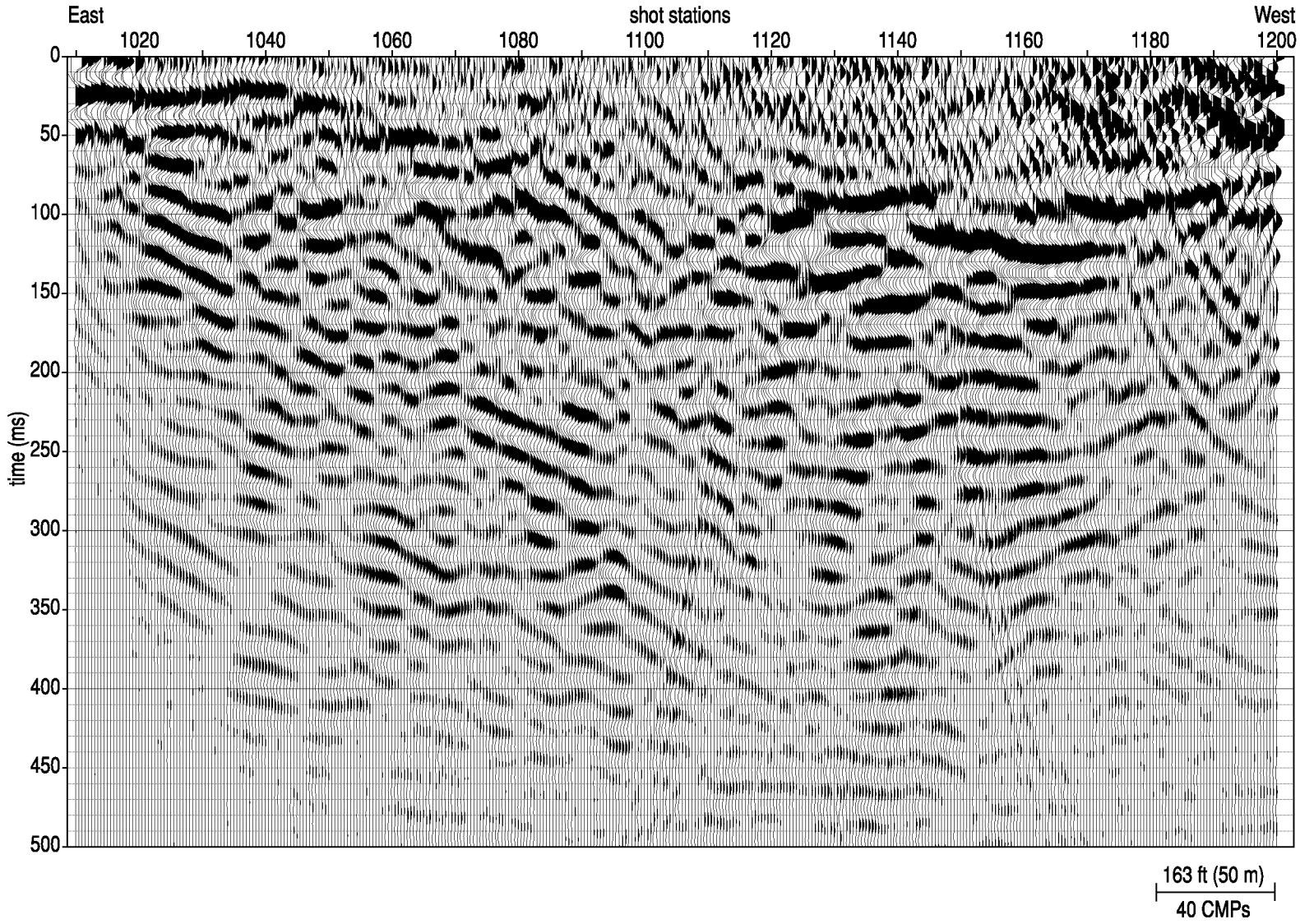

Figure 61. Migrated compressional-wave CMP-stacked section along the north abutment road.

Several key characteristics and types of arrivals, evident on the CMP stacked section, are worth noting (Figure 61). First, a series of relatively high-amplitude coherent arrivals with a significant left to right (east to west) dip are consistent with the expected arrival pattern of diffracted energy. For these data several apexes can be identified that could possibly be representative of subsurface scatter points. The most pronounced of these include data from beneath stations 1025, 1065, and 1100. Second, artifacts of the migration processing show up as curved, coherent wave trains, very closely resembling water waves radiating outward from a pebble dropped in an otherwise still pond.

The shallowest coherent events, especially on the east end of the survey, could be direct or refracted energy (Figure 61). During pre-CMP stack processing first arrivals were muted several zero crossings after the first arriving source generated seismic energy. It is possible that the first arrivals were not completely eliminated and this shallow event is a remnant of linear body waves. Scaling applied to these data have resulted in the appearance of strong background noise prior to first-arriving source energy on the western end of the profile. This noise is disproportionately amplified by the gaining process.

Correlating these compressional-wave CMP-stacked data from the abutment with those from the toe line allows some very interesting observations (Figure 62). Using borehole-measured average velocities for both sections it appears that the toe line matches quite well with the eastern half of the abutment line. On the abutment line only one coherent event can be interpreted with any degree of confidence as a reflection. The deeper event interpreted on toe data are within the coherent-noise area that appears to be dominated by scattered energy from around station 1020. Beneath station 1040 on the abutment line there does appear to be a second arrival that matches very well with the second arrival on the toe line. Events interpreted in red on these figure are possible reflections but not the target of the survey. Yellow events are, at this preliminary stage of geologic correlations, interpreted as the basal contact of the conglomerate with the suspected underlying shale. Considering the difference in elevation of the two lines and the dip observed in outcrop, it is reasonable to suggest around a 200 ft difference in the same reflector imaged on both the toe and crest profiles.

Three distinct areas on the CMP stacked data can be identified based on seismic character and coherent-event arrival patterns (Figure 62). As previously discussed, the eastern third of the survey line is defined by what appear to be coherent events with character and geometry consistent with reflections. Also prominent on this portion is scatter energy with extremely uniform phase velocity. The middle one-quarter of the section possesses high-dip angle semi-coherent events with little in the way of even potential reflection events. Nearly half of the western section is characterized by mostly flatter events with a much deeper first coherent event. Another distinguishing characteristic of these data is the NMO velocity at which these events flatten best. East of about station 1085 the velocity is quite high relative to the NMO velocity necessary to flatten curved events west of station 1120. Quite distinctive on shot gathers is the significant increase in extremely low-velocity material above rock beyond station 1120. This is seismically evident in the direct and refraction intersection or cross-over.

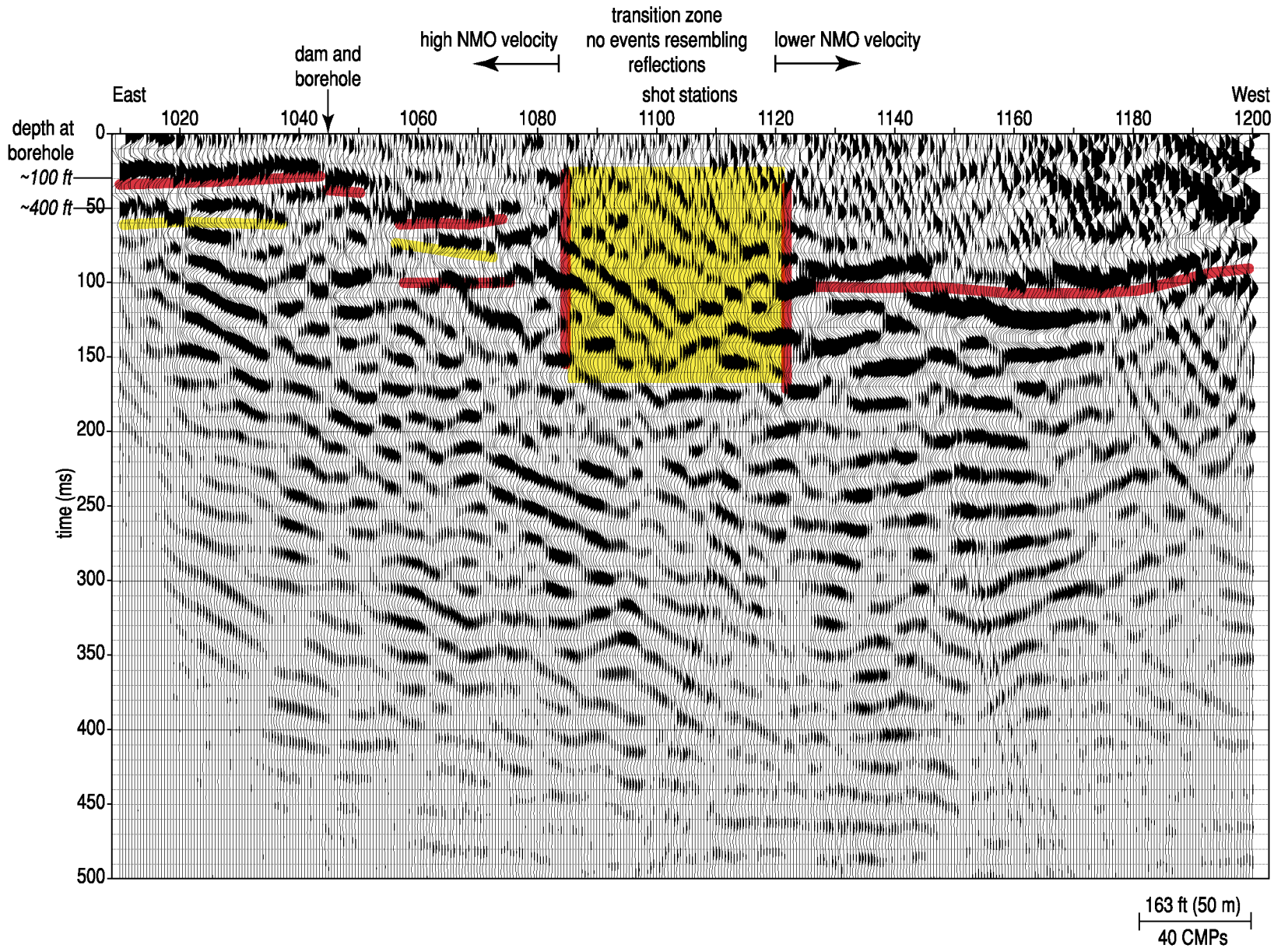

Figure 62. Migrated compressional-wave CMP-stacked section along the north abutment road.

Shear

Shear-wave shot gathers from along the abutment line are similar to compressional-wave shot gathers with respect to the lateral inconsistency in wavelet characteristics and the multitude of high-angle dipping events likely the result of scattered body-wave energy (Figure 63). An apparent reflection-looking event is between receiver station 1070 and 1120 at a depth of around 225 ms. With this event being outside the noise cone there is no chance it is related to the dispersive appearance of surface-wave energy at close offsets (a problem commonly plaguing shallow shear-wave reflection data) (Miller et al., 2001). Another possible event can be interpreted at about 200 ms on the eastern end of the shot gather. In general, between statics and scattered energy it is difficult to confidently interpret a continuous reflection event on shot gathers.

The CMP-stacked shear-wave section as well grossly resembles the compressional-wave stacked section (Figure 64). On the extreme eastern portion of the stacked section a series of relatively flat events are evident. These events dip significantly to the west, until they encounter a transition zone at approximately the same stations as observed on compressional-wave stacked sections. On the western end of the profile the events are relatively flat and even appear in some places to dip a bit to the east. Dominant frequency of these stacked data is a bit lower than

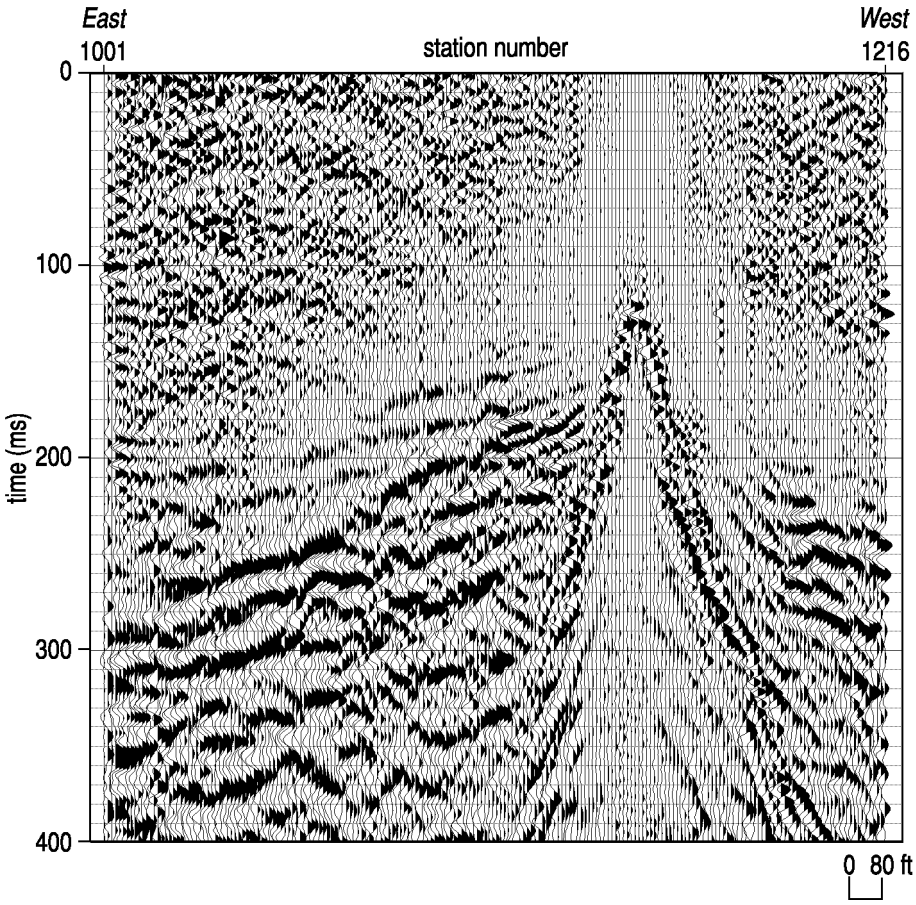

Figure 63. Shear-wave shot gather with the vibrator in SH mode. A subtle indication that reflection energy is being recorded can be seen at around 220 ms. This event is outside the ground cone, therefore is not aliased surface wave.

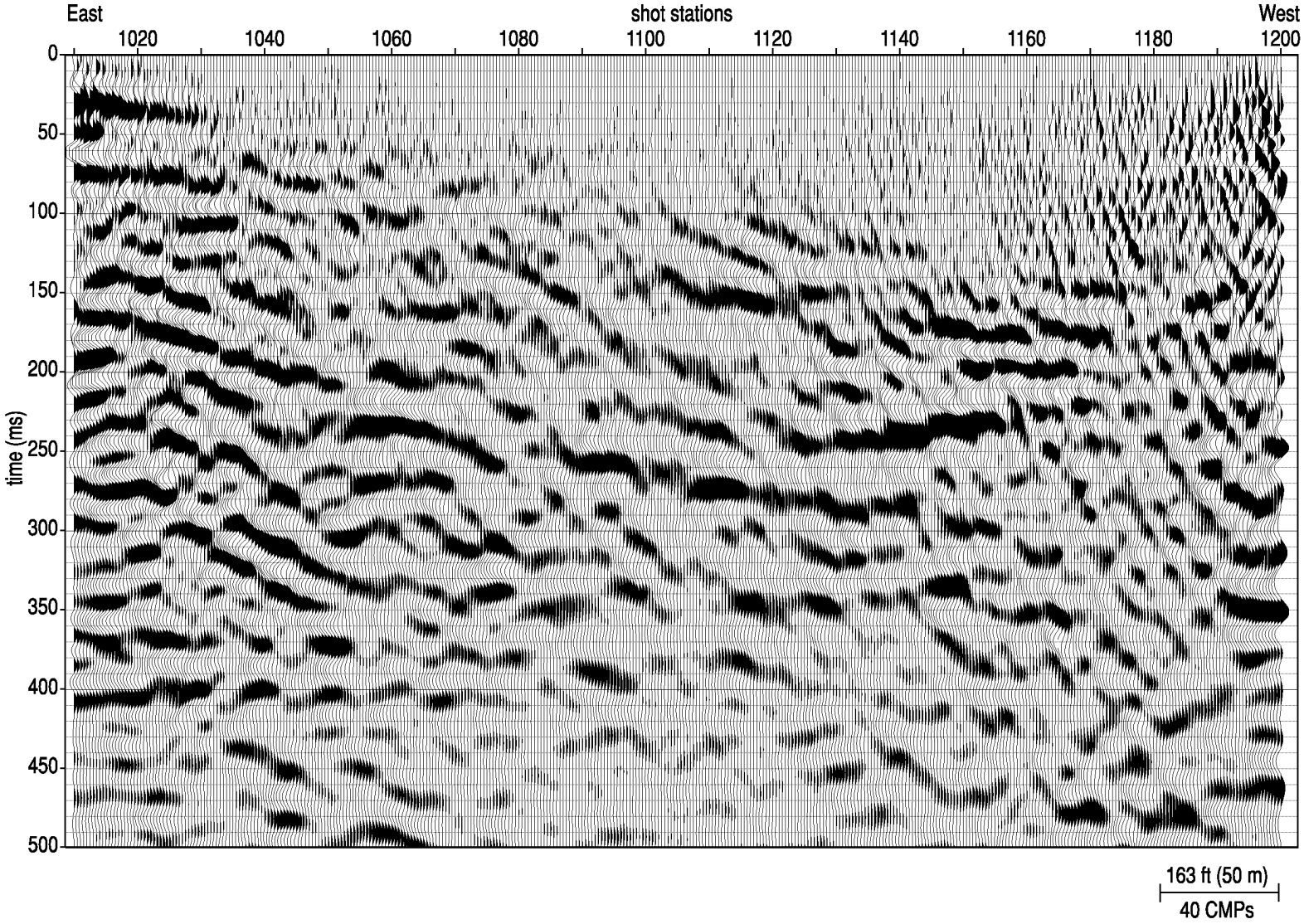

Figure 64. Migrated shear-wave CMP-stacked section along the north abutment road.

compressional-wave data, but that is to be expected considering the propagation characteristics of shear- versus compressional-wave energy.

Interpretations of the CMP stacked shear-wave section are also quite consistent with both the compressional-wave data from along this line and the shear- and compressional-wave data from the toe (Figure 65). Events interpreted in red are coherent events that could be reflection, but not the focus of these interpretations. The event highlighted in yellow was selected based on correlation with other data and estimates based on local geology as to the most feasible event to represent the basal contact of the massive conglomerate exposed at the surface and acting as the foundation for the dam. Depth estimates are based on average velocities measured in the crest borehole located off-line approximately 125 ft and immediately adjacent to station 1045. With the shear-wave velocity being 50% slower than the compressional-wave velocity the apparent resolution is higher for the shear than the compressional, and the interpreted events appear to have more dip as a direct consequence of lower shear velocity while display parameters were maintained (trace and time scales).

East of station 1080 on the CMP shear-wave stacked section the depth profile is quite consistent with that suggested for the toe line (Figure 65). If the yellow event is the basal contact of the conglomerate, at station 1045 (coincident with the borehole) the contact would be around 600 ft BGS. On equivalent shear-wave data from the toe the basal contact of the conglomerate was estimated to be around 350 ft. Considering the height of crest borehole is around 200 to 250 ft greater that than the toe, it seems logical these seismic events are from the same geologic feature. Again a zone with geologically unfeasibly steep dips is interpreted between stations 1080 and 1120. West of station 1120 the events are flatter and quite consistent with similar depth events interpreted on the compressional-wave profile.

Borehole

On the crest the borehole was drilled directly through the concrete dam and into the rock approximately 53 ft below the top of the dam at the drill location. Since the dam was only wide enough for one source at a time, one source was positioned at the close-offset (near-vertical VSP) location while the other source was positioned at the far-offset location (offset VSP). Therefore, for each run from the bottom of the borehole to the surface with the receivers, one mode of close-offset was recorded with the other mode at longer offset. Using this deployment approach the borehole receiver only had to traverse the hole twice to get data from both sources for each subsurface sampling location. Longitudinal data were acquired with the source and receiver oriented with their axis of sensitivity parallel to the centerline of the dam crest. Transverse data were acquired with both source and receiver polarized to be most sensitive to particle displacement perpendicular to the main axis of the dam.

A major obstacle and deterrent to a high-quality borehole survey at this location was the extreme noise produced by the outlet works valve at high-volume discharges during data acquisition. The noise produced by the water moving through the dam and splashing against the rocks in the stilling basin was obvious on data and required both increased stacking during acquisition and more aggressive data processing than would have been preferred. Vertically stacking data to enhance signal requires excellent timing and is rarely possible to the degree necessary for interval-velocity selections when picking first arrivals from borehole data. Slight

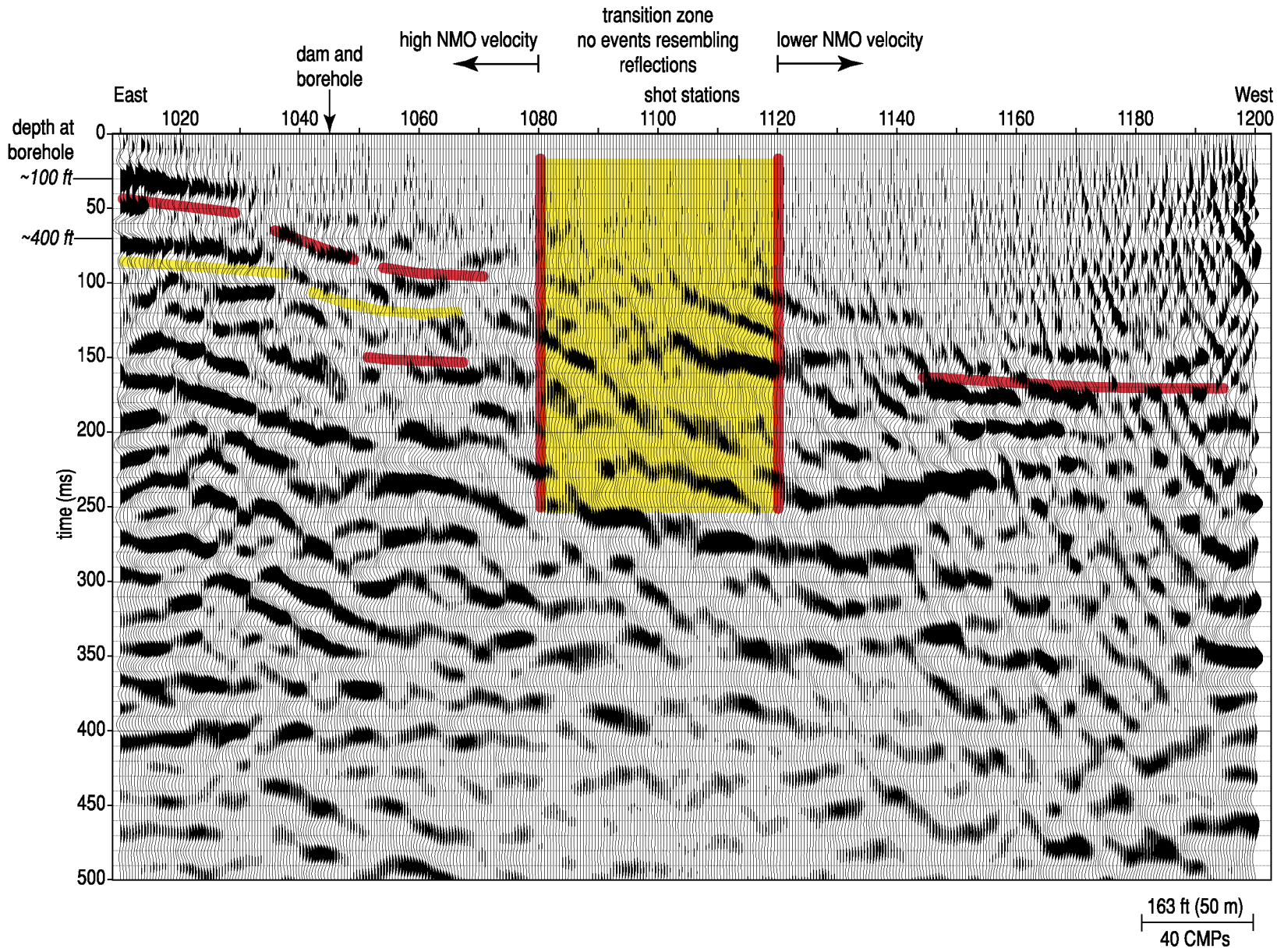

Figure 65. Migrated shear-wave CMP-stacked section along the north abutment road

(0.125 ms) variability in wavelet properties or timing will degrade the spectra of the stacked wavelet and can adversely influence selections of first-recorded energy.

Downhole

Near-vertically incident ray paths between source and receiver were used to estimate average velocity between the crest of the dam and the receivers incrementally moved up the borehole between about 10 ft and 240 ft BGS (Figure 66). First-arriving energy is represented as a minimum-phase wavelet for compressional-wave data and zero-phase for shear data. This difference basically dictates where the zero time or timed arrival of the fastest energy mode is defined. Ideally, with the three-pod configuration of this tool, interval velocities could be more confidently measured opposed to a single pod, which incorporates source static as another source of error. A lack of a sufficiently consistent wavelets and tool malfunction (clamping device failed on two pods toward end of survey in crest borehole) prohibited direct measure of interval velocity using this single tool, multi-pod approach.

Compressional-wave first arrivals are quite sharp, allowing very confident picks (Figure 67). Early arrivals appear at two different depth horizons (approximately 90 ft BGS). This can be seen on both the shot gather and the average-velocity plots (Figure 68). The source of these errant arrivals is not clear, but considering the interval velocity that would be necessary for this to be a real value, the most likely cause must be related to the acquisition process. Several possible reasons exist for such an erratic, including receiver location or coupling and time break (time zero signal from the source). Average velocities within the borehole are relatively uniform increasing from around 6000 ft/sec within the concrete of the dam to near 15,000 ft/sec at 250 ft BGS.

Shear-wave first arrivals on close-offset data lack the uniformity of the compressional-wave data, a characteristic associated with vibroseis data and the increased difficulty coupling a shear source (Figure 66). Of particular interest on the shear-wave first-arrival data are two distinctive features. First, on the N/S (longitudinal) orientation between about 150 ft and 170 ft BGS, first-arrival wavelets get very inconsistent and lack the more impulsive nature observed on other first arrivals deeper and shallower (Figure 69). From borehole geological logs this interval possess a unique lithology than the average for this hole. A similar abnormality can be observed on the E/W (transverse), but it takes a completely different form in comparison to the N/S data. This sensitivity of only the longitudinal component of the shear energy to this change in lithology is very suggestive of layer orientation, especially related to fractures. Second, at the concrete/rock contact the E/W first-arrival wavelet changes dramatically. This change in wavelet is only observed on the transverse data; neither the compressional or longitudinal have any indication a change in material occurs at 53 ft BGS.

These rocks have very evident anisotropic characteristics. The two shear-wave measurements do suggest faster- and slower-velocity directions are prevalent for specific depths and tool orientations (Figure 68). It is difficult within the dam to suggest the difference in the two polarized shear-wave energy arrivals is related to anisotropy or simply the lack of uniformity in the wavelet due to the extreme geometry of the dam. Considering the wavelength of the shear energy within the dam is around 60 ft and the transverse (E/W) or cross-sectional direction relative to the dam's axis is only 20 ft wide at its maximum, the transverse energy wavelet will

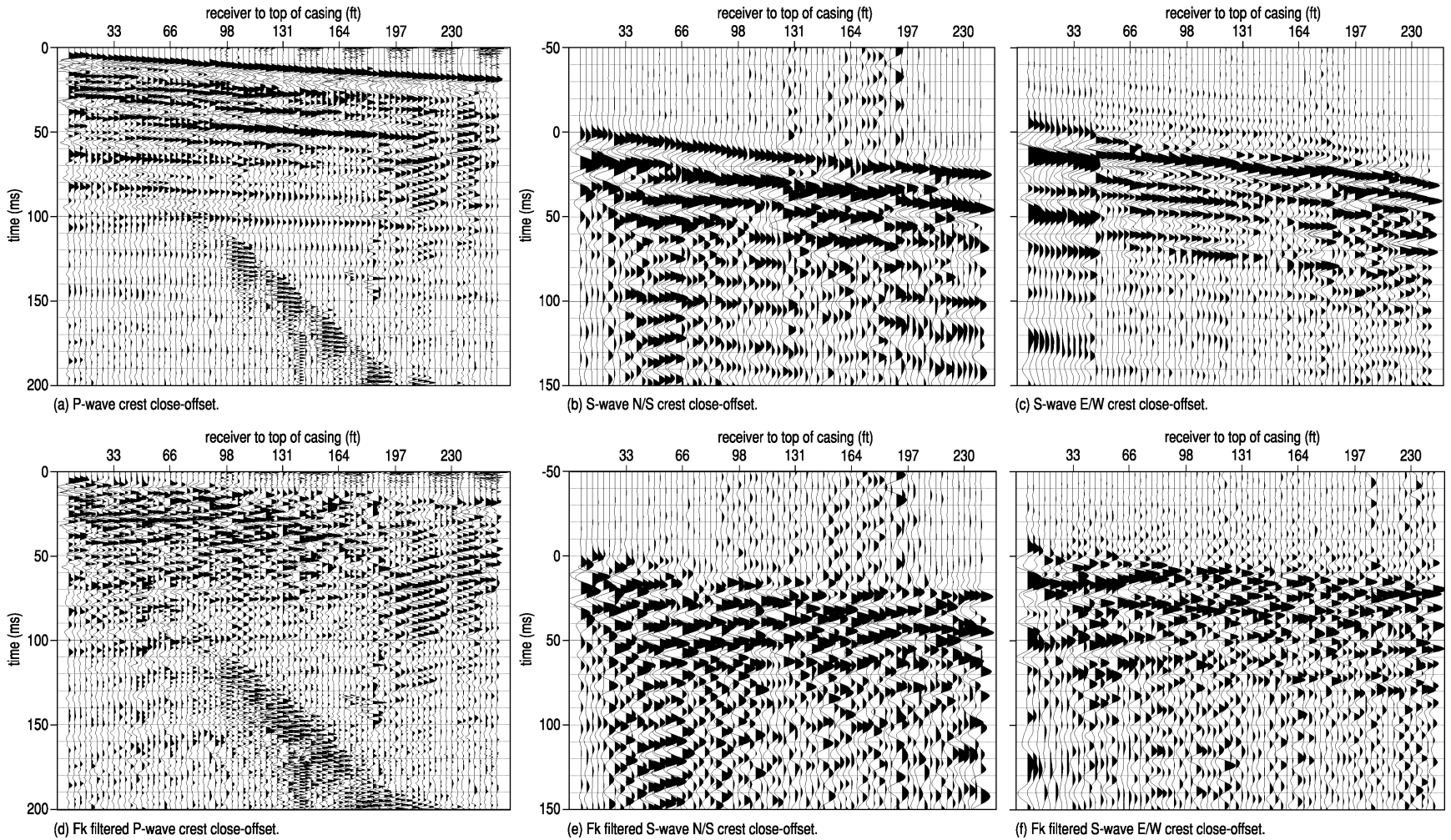

Figure 66. Close-offset VSP/downhole data acquired with the three-component three-pod downhole geophone system using the RAWD for compressional-wave (a) and (d) and IVI minivib shear wave for shear-wave data (b), (c), (e), and (f).

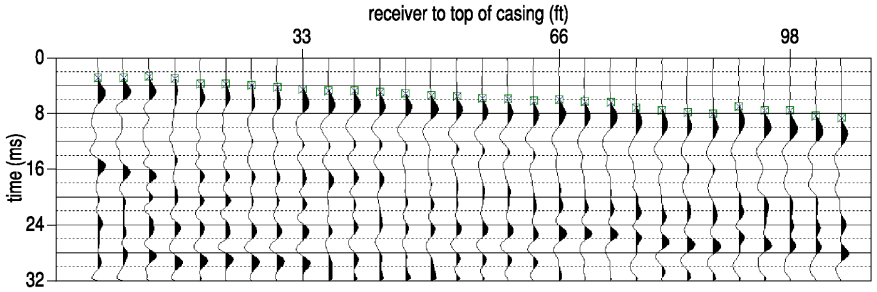

Figure 67. Compressional-wave gather of close-offset VSP raw data from crest borehole. Consistency in first-arrival wavelet allows good confidence in selecting the instantaneous onset of energy.

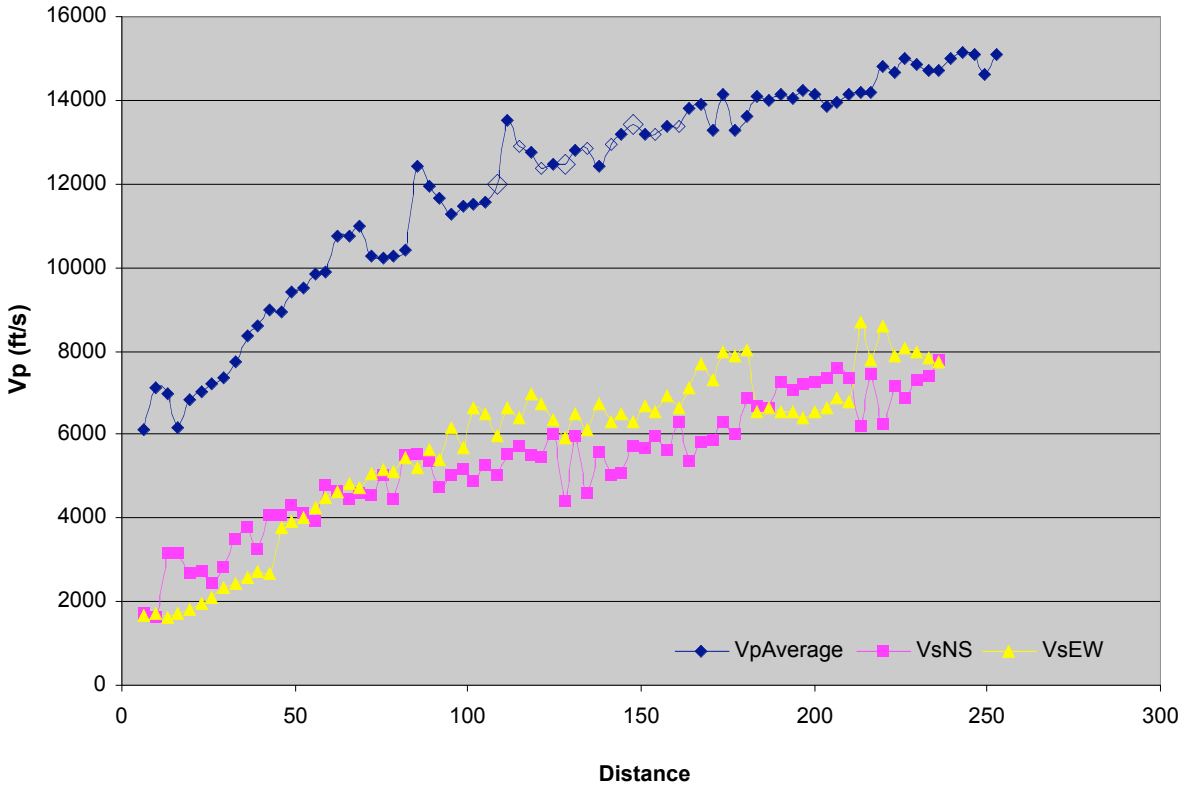

Figure 68. Average velocities measured in crest borehole.

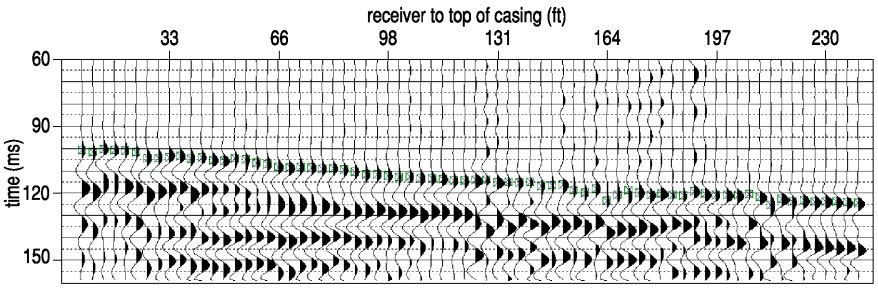

Figure 69. VSP data from crest recorded by longitudinal geophones when source was also in line with the dam axis. First arrivals are selected at maximum value of the first peak, since these are vibroseis data and the source wavelet is zero phase.

never fully develop within the dam and the dam will effectively operate as a wave guide to the detriment of full wavefield analysis.

Looking below the concrete/rock contact defining the dam geometry, subtle differences in shear-wave velocity can be identified and very qualitatively defined (Figure 68). From about 80 ft BGS to 180 ft BGS the longitudinal component of the shear wave is about 10% slower than the transverse. In locations within the borehole this difference drops to near 0%, but on the average it clearly appears as though the N/S orientation is slower. Interesting is a zone between about 180 ft and 210 ft BGS where the opposite is true. The degree of anisotropy is much less, around 5%, but still quite pronounced over that interval. Throughout the entire borehole interval from about 80 ft to the last seismic measurement at around 240 ft BGS are clear indications of anisotropy with varying degrees of slowness and orientation.

With the good quality of the borehole first-arrival data, it is possible to make several observations about average and interval velocities (Figure 68). First, comparison of average shear and average compressional suggest an interesting change in the structural properties of the rock relative to the dam. Ratio of Vp and Vs in the shallowest 50 ft is around 2.2 to 2.5 while moving to around 125 ft BGS the ratio decreases to around 2.0 and at 225 ft BGS the Vp/Vs is around 1.75. This gradual decrease in Vp/Vs between the dam and native foundation material suggests the rock is stiffer or more rigid than the concrete by a sizeable amount.

Going the next step and attempting to estimate interval velocity was not particularly successful. With subtle inconsistencies in selecting the instant seismic source energy arrived at the receiver due to timing, vertical stacking, and noise issues, interval velocities can only be qualitatively estimated and discussed over larger intervals (several to ten receiver station averages). For compressional-wave data abrupt jumps in interpreted first-arrival times clearly show up on average-velocity estimates as erroneous increases or decreases in velocity that result in unrealistic interval velocities (Figure 70). Looking at trend-based averaging of larger intervals two areas show up with anomalously low interval velocities. These depth ranges are from about 150 ft to 160 ft BGS and 200 ft to 215 ft BGS. Both of these two areas also show up on sonic logs as low-velocity zones. These two low-velocity zones are evident but not as pronounced on shear-wave data (Figure 71).

VSP

These data do not lend themselves to VSP analysis. A combination of geology, limited offset opportunities, and noise (geologic and cultural) make extending these data beyond check shot and qualitative observations impractical. However, several very interesting observations concerning unique arrivals and arrival patterns on these data do provide nuggets of information that can be incorporated into sitewide geologic models of the area. All three components from both offsets were fk filtered in an attempt to remove all downgoing energy (Figures 66 and 72).

Compressional-wave data are much higher frequency than shear, as expected, and possess arrivals that appear to have reflection properties on close-offset data (Figure 66). Longer-offset compressional data do not possess these same characteristics, likely as a result of

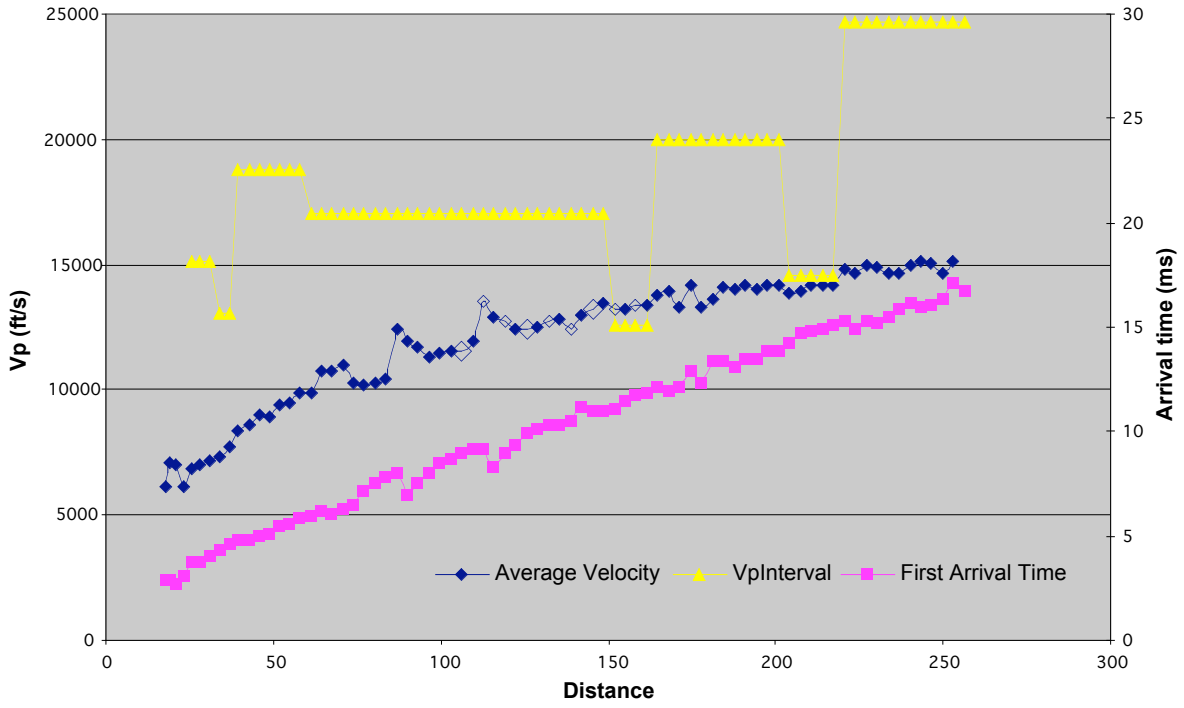

Figure 70. Measure of first-arrival times and calculations of average and interval (over several receiver stations) velocity for compressional-wave data.

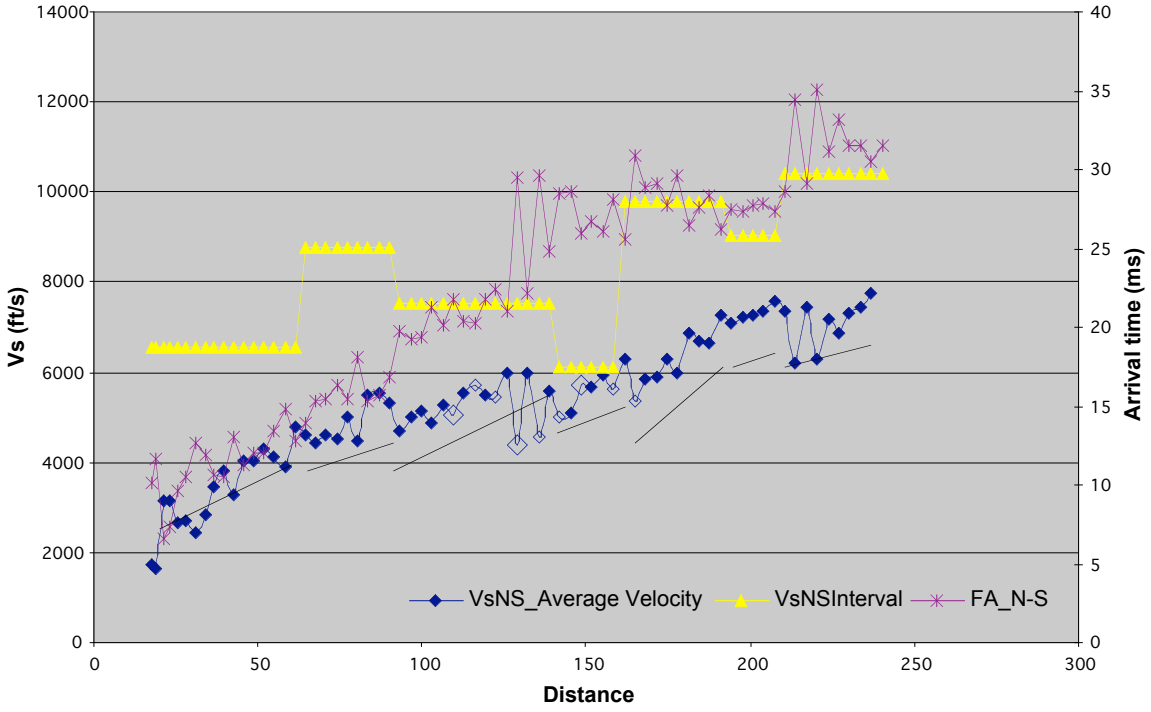

Figure 71. Measure of first-arrival times and calculations of average and interval (over several receiver stations) velocity for shear-wave data.

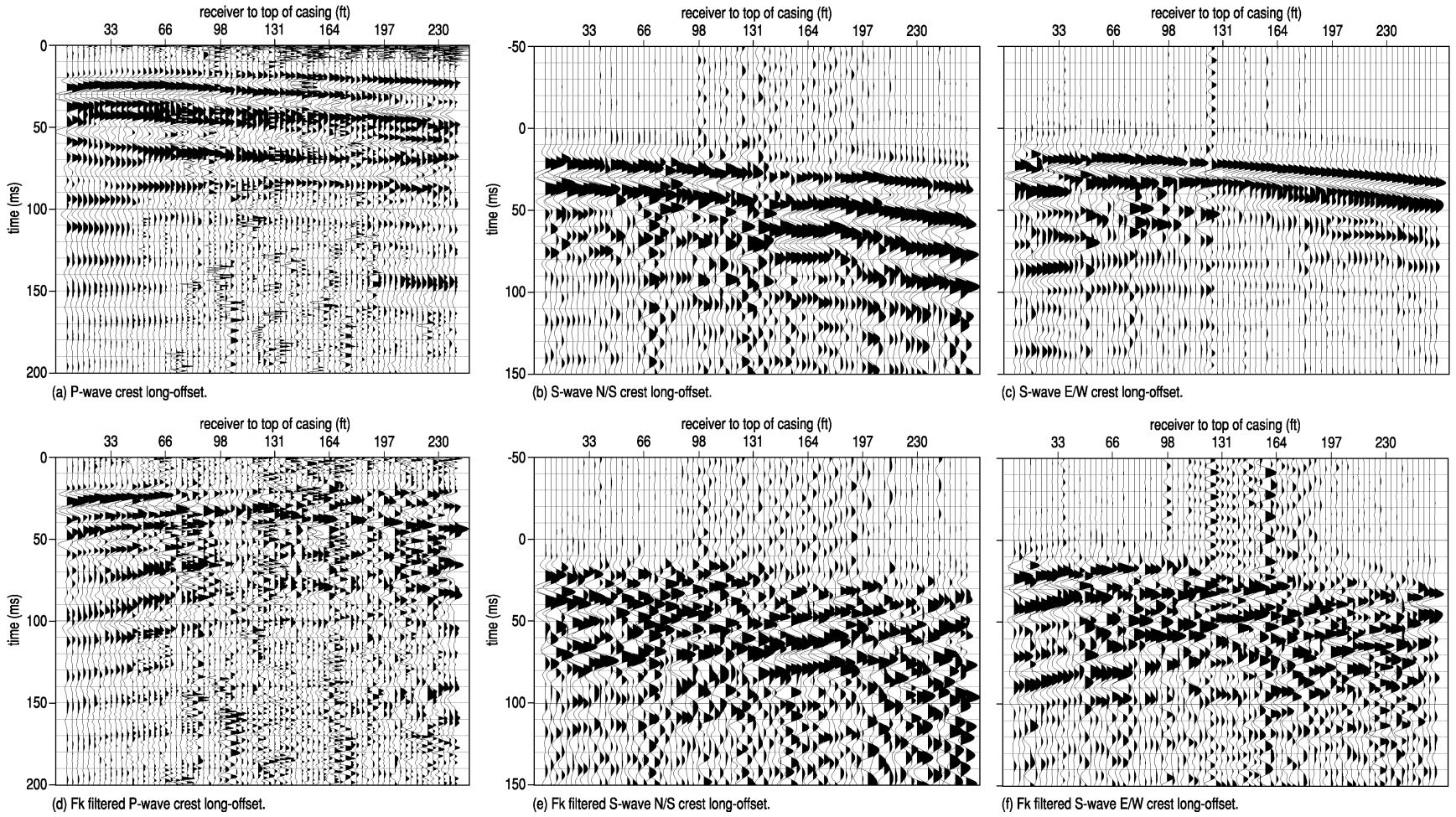

Figure 72. Borehole shot gathers with source offset around 140 ft from borehole and fk-filtered gathers attempting to remove all downgoing energy.

the dipping geology and relative orientation of the offset source station and borehole. A series of cyclic, high frequency arrivals observable at deeper receiver stations are clearly up-going energy, likely originating from a substantial interface or point source (Figures 66a and 66d). Most other events with slopes appropriate for up-going energy are extremely questionable candidates for reflections due to an inverted amplitude-depth relationship. Basically the largest amplitudes of coherent events with reflection slopes are at the shallowest receivers, implying a positive amplitude growth with increased travel path.

Closer-offset shear-wave VSP data have several unique characteristics worth mentioning (Figure 66). First, as pointed out during downhole discussions, the transverse shear data set have a strong signature associated with the dam relative to the native rock (Figure 66c). Also, the longitudinal data appear to have a very ringy series of arrivals resembling scatter with upcoming phase-velocity orientation (Figure 66e). If the borehole would have been water filled these cyclic arrivals with upcoming-wave directionality would be a strong candidate for tube generated at a fracture or discontinuity exposed in the borehole. The origin of this ringy series of arrivals is about 66 ft BGS within the borehole. This same feature is also evident on longer-offset compressional-wave data originating from around 70 ft BGS in the borehole (Figure 72d). No evidence of this ringy series of events can be detected on the transverse data set at either offset.

Longer-offset VSP data generally provide the best environment (offset range vs depth of interest and associated incident angles of downgoing and upcoming rays) for recording reflections (Figure 72). Considering attenuation, the highest amplitudes on reflected events should be where the reflector intersects the borehole. Therefore, dipping events with highest amplitudes at the shallowest depths and greatest distance from the trace where intersection of the direct and reflected energy occurs are likely fk artifacts or out-of-the-plane noise events. Careful study of the shear-wave data at greater depths in the borehole suggests reflections might have been recorded from beneath the bottom of the borehole. Both longitudinal and transverse fk-filtered data possess an event with “reverse dip” (increasing in time from left to right or bottom to top) that comes from beneath the deepest-receiver sample point. This event does not have the pronounced characteristics that would allow confident correlation with CMP stacked reflection sections.

Velocity anomalies associated with a potential fracture zone between about 140 ft and 170 ft BGS is interpretable on the longitudinal data (Figure 72b). This apparent lower-velocity zone is consistent with a similar reduction in the interval velocity on close-offset data (Figure 66). Close-offset compressional-wave data (Figures 66a and 68) possessed a pronounced drop in velocity that generally correlates with an observed velocity change on sonic data (Figure 34).

Considering the geometry of the dam and foundation it is difficult to say whether any of the information recorded on the VSP data were from reflections beneath the bottom of the borehole or from portions of the exposed rock face or fractures observed in outcrop with every imaginable orientation or even energy that has taken an indirect route interacting with multiple discontinuities along the way. Clearly the geology has had a major impact on how well this VSP can be correlated to geology.

Frequency Dwell

In an attempt to determine if and how seismic energy might be altered crossing the dam/rock interface, energy from the acentric vibrator at incremental frequencies was recorded on the three-pod, three-component geophones with the center pod at the contact between dam and rock. With the center pod straddling the concrete/rock interface, the upper pod was recording data from the dam and the lower pod was recording seismic energy from the rock (Figure 73). Measurements were made by Bureau of Reclamation staff using the acentric vibrator and several accelerometers placed along the dam crest access road. These measurements were intended to evaluate resonance effects in the dam.

To get a better understanding of how energy is affected by the concrete/rock interface, the borehole receiver system was manually triggered and set-up to record for 10-second periods coincident with each unique frequency setting of the acentric vibrator. A new record was recorded for each increment in vibrator frequency. Shear waves are the predominant energy generated by the acentric vibrator and therefore the highest-amplitude data are expected from shear-wave receivers. Analysis of these data focused on amplitude/frequency relationships. Therefore spectral analysis was done on each trace, taking care to maintain the true amplitudes needed for display and comparison. A shot gather was recorded each time the eccentric vibrator was incremented 0.1 Hz resulting in approximately 70 shot records each at a unique constant dwell frequency.

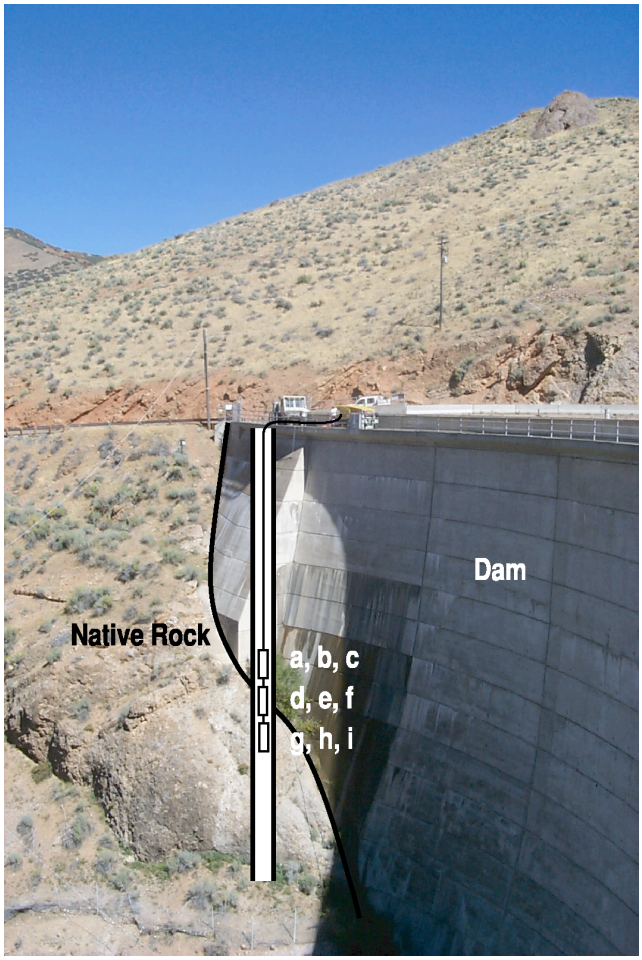

Figure 73. Graphic/pictoral representation of dwell experiment. Alpha characters relate to parts of Figure 74.

Considering previous discussions of VSP data, it is reasonable to expect longitudinal shear to be the highest-amplitude mode recorded, followed by transverse shear, with compressional-wave data recorded at the lowest energy level. Comparison of the nine different receivers matches that expectation (Figure 74). Interesting to note is that longitudinal shear energy is transmitted through the concrete of the dam at 12 dB higher levels than transverse. An overwhelming majority of the compressional-wave energy generated by the eccentric vibrator and propagated through the dam structure is the result of mode conversion. Compressional-wave data recorded in the dam are over 30 dB lower amplitude than longitudinal shear.

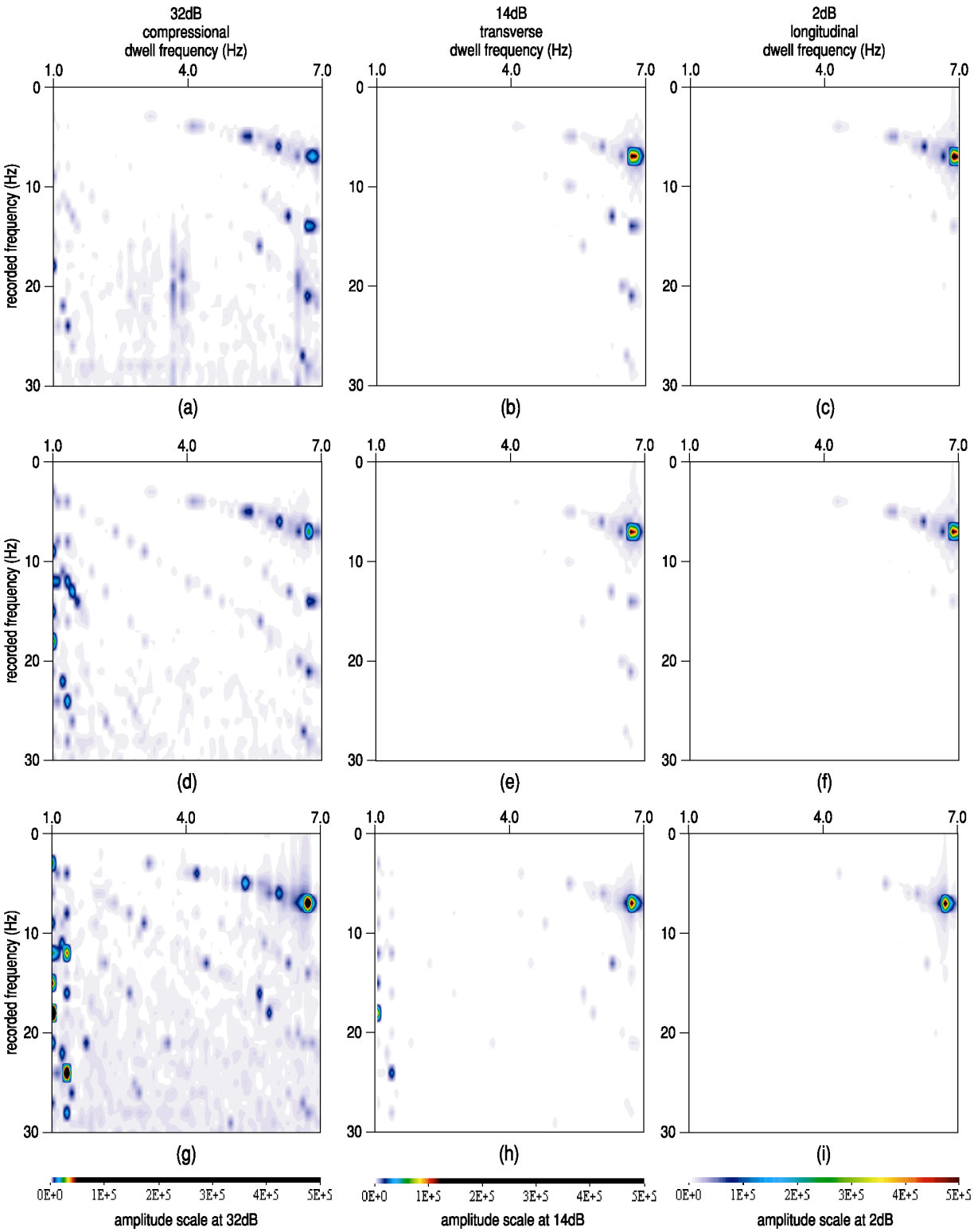

Figure 74. Amplitude variations with frequency of compressional geophone (a), transverse-shear geophone (b), and longitudinal-shear geophone (c) from the dam; compressional geophone (d), transverse-shear geophone (e), and longitudinal-shear geophone (f) at the concrete-rock contact; and compressional geophone (g), transverse-shear geophone (h), and longitudinal-shear geophone (i) from the rock.

Breaking down the data a bit further, it appears the resonant frequency in the dam is between 6.8 Hz and 6.9 Hz (Figure 74). Two observations can be made concerning this resonance phenomena. First the resonant frequency for longitudinal energy within the dam is about 6.9 Hz, while it is around 6.8 Hz for transverse shear. Also noteworthy is the resonance of compressional-wave data is 6.8 Hz in the dam as well as in the rock. In the rock the resonance of shear energy (both longitudinal and transverse) is around 6.8 Hz. This leads to the statement that resonance in the dam is modal dependent, while within the rock there appears to be no dependence on mode. If this observation is correct, the boundary between the concrete and rock acts to excite different frequencies of longitudinal energy as it passes through the contact zone without significantly attenuating the overall energy level of that mode.

Interesting to note are changes in resonant-frequency amplitude of the various modes after passing through the concrete/rock contact. Besides changing resonant frequency the longitudinal energy level at around 6.8 Hz is lower below the interface in compared to in the concrete by a small amount (Figure 74). As well, both the amplitude and the bandwidth of the resonance phenomena for the transverse shear mode have decreased slightly. Probably most interesting is the notable increase in amplitude of the compressional-wave energy below the contact.

Reduction in energy levels such as seen here can be explained through attenuation across the concrete/rock boundary. It is even possible to conceive changes in frequency are possible during the transition from concrete to rock, but an increase in amplitude is counter-intuitive unless shear energy loss is at least in part due to mode conversion across the interface (shear loss is compressional gain). No doubt some of the amplitude drop in the rock relative to concrete is due to transmission loss across the interface, but there appears to be no other reasonable explanation for the increase in compressional energy except mode conversion at the interface. These observations suggest energy moving across this interface will experience notable changes in properties in the concrete relative to in the rock.

Conclusions

None of the methods investigated here worked up to their full potential. In part this is related to the extremely difficult geologic setting and abundant noise present on this site. The dipping conglomerate with a multitude of local fractures, in association with the steep cliff face along which the seismic reflection was acquired, provided excellent scatter and out-of-the-plane reflection sources. Even with these obstacles, reflections appear to have been recorded and by looking only at dip-specific directional data it is possible to interpret a discontinuity at depths of around 400 or so feet near the dam, deepening in the downstream direction. A marked change in near-surface material is also evident from about 400 ft downstream and continuing in the downstream direction. Reflections interpreted on all four seismic sections (P and S from toe and abutment) have character similarities that with some degree of skepticism can be correlated between lines.

VSP data suggest several intervals where velocity variations (likely associated with fractures) are present, but the only confident reflection appears to come from depths beneath the bottom of the borehole. This reflecting event is likely the basal contact of the conglomerate, which was speculated to be observed on the CMP reflection data. It can also be suggested from

these data that some shear-wave anisotropy exists within the conglomerate rock column. Bore-hole sonic measurements suggest a marked change in shear velocity at the conglomerate/concrete contact.

MASW and turning-ray tomography both suggest a low-velocity veneer of weathered conglomerate overlays a very high-speed conglomerate. Dipping layers (more likely bedding planes) defined by high concentrations of fractures as observed in outcrop are represented on the toe profiles as less resistant zones which possess lower seismic velocities. A very irregular weathered/unweathered layer topography appears consistent with the cycles of these fractures observed both in the road cut near the crest and in the valley walls near the outlet works. Changes in velocity that appear to be related to more or less erosionally resistant zones within the rock have a pinnacle-looking appearance. Dipping and associated subcrop of unweathered conglomerate are evident on tomography data as shingling of high-velocity slabs with an apparent dip consistent with surface exposures.

REFERENCES

Carmichael, R.S., ed., 1989, Practical handbook of physical properties of rocks and minerals: CRC Press, Boca Raton, Florida.

Cottin, J.F., P. Deletie, H. Jacquet-Francillon, J. Lakshmanan, Y. Lemoine, and M. Sanchez, 1986, Curved ray seismic tomography–Application to the Grand Etang Dam (Reunion Island): *First Break*, v. 4, no. 7, p. 25-30.

Crawford, J.M., W.E.N. Doty, and M.R. Lee, 1960, Continuous signal seismograph: *Geophysics*, v. 25, p. 95-105.

Ghose, R., 2002, High-frequency shear wave reflections from shallow subsoil layers using a vibrator source: Sweep cross-correlation versus deconvolution with groundforce derivative [Exp. Abs.]: Soc. Explor. Geophys., p. 1408-1411.

Glover, R.H., 1959, Techniques used in interpreting seismic data in Kansas: In *Symposium on Geophysics in Kansas*, ed. W.W. Hambleton. Kansas Geological Survey Bulletin 137, p. 225-240.

Haeni, F.P., 1978, Computer modeling of ground-water availability in the Pootatuck River valley, Newtown, Connecticut, with a section on quality of water by Elinor H. Handman: U.S. Geological Survey Water Resources Investigations Open-file Report 83-4221.

Hardage, B.A., 1983, Vertical seismic profiling, Part A–Principles: Geophysical Press.

Hunter, J.A., S.E. Pullan, R.A. Burns, R.M. Gagne, and R.L. Good, 1984, Shallow seismic reflection mapping of the overburden-bedrock interface with the engineering seismograph–Some simple techniques: *Geophysics*, v. 49, p. 1381-1385.

Ivanov, J., 2002, JASR – Joint analysis of surface waves and refractions. Ph.D. dissertation, University of Kansas.

Kilty, K.T., and A.L. Lange, 1990, Acoustic tomography in shallow geophysical exploration using a transform reconstruction: Soc. Explor. Geophys. Investigations in Geophysics no. 5, S.H. Ward, ed., *Volume 3: Geotechnical*, p. 23-35.

Lytle, R.J., and K.A. Dines, 1980, Iterative ray tracing between boreholes for underground image reconstruction: Inst. Electr. Electron. Eng. Trans. Geosci. Remote Sensing, v. GE-18, p. 234-240.

Mayne, W.H., 1962, Horizontal data stacking techniques: Supplement to *Geophysics*, v. 27, p. 927-938.

Miller, R.D., 1992, Normal moveout stretch mute on shallow-reflection data: *Geophysics*, v. 57, p. 1502-1507.

Miller, R.D., and D.W. Steeples, 1991, Detecting voids in a 0.6-m coal seam, 7 m deep, using seismic reflection: *Geoexploration,* Elsevier Science Publishers B.V., Amsterdam, The Netherlands, v. 28, p. 109-119.

Miller, R.D., D.W. Steeples, and M. Brannan, 1989, Mapping a bedrock surface under dry alluvium with shallow seismic reflections: *Geophysics,* v. 54, p. 1528-1534.

Miller, R.D., D.W. Steeples, and P.B. Myers, 1990, Shallow seismic-reflection survey across the Meers fault, Oklahoma: *GSA Bulletin*, v. 102, p. 18-25.

Miller, R.D., T.S. Anderson, J.C. Davis, D.W. Steeples, M.L. Moran, 2001, 3-D characterization of seismic properties at the Smart Weapons Test Range, YPG: Proceedings of the Military Sensing Symposium on Battlefield Seismic and Acoustic Sensing, October 23-25, Laurel, Maryland, Published on CD.

Miller, R.D., J. Xia, and C.B. Park, 2001, Love waves: A menace to shallow shear wave reflection surveying [Exp. Abs.]: Soc. Expl. Geophys., p. 1377-1380.

Miller, R.D., J. Xia, C.B. Park, and J.M. Ivanov, 1999, Multichannel analysis of surface waves to map bedrock: *Leading Edge*, v. 18, n. 12, p. 1392-1396.

Mooney, H.M., 1981, Handbook of engineering geophysics: Bison Instruments, Inc.

Nazarian, S., K.H. Stokoe II, and W.R. Hudson, 1983, Use of spectral analysis of surface waves method for determination of moduli and thicknesses of pavement systems: Transportation Research Record No. 930, p. 38-45.

Palmer, D., 1980, The generalized reciprocal method of seismic refraction interpretation: Soc. of Expl. Geophys., 104. (Edited by K.B.S. Burke.)
Park, C.B., R.D. Miller, D.W. Steeples, and R.A. Black, 1996, Swept impact seismic technique (SIST): *Geophysics*, v. 61, p. 1789-1803.
Park, C.B. R.D. Miller, and J. Xia, 1999, Multichannel analysis of surface waves (MASW): *Geophysics*, v. 64, p. 800-808.
Park, C.B., R.D. Miller, and J. Ivanov, 2002, Filtering surface waves: Symposium on the Application of Geophysics to Engineering and Environmental Problems (SAGEEP 2002), Las Vegas, Nevada, February 10-13, Paper 12SEI9, published on CD.
Peterson, J.E., B.N.P. Paulsson, and T.A. McEvilly, 1985, Applications of algebraic reconstruction techniques to cross-hole data: *Geophysics*, v. 53, p. 1284-1294.
Redpath, B.B., 1973, Seismic refraction exploration for engineering site investigations, NTIS AD-768710.
Sander, J.E., 1978, The blind zone in seismic ground-water exploration: *Ground Water*, v. 165, p. 394-397.
Schepers, R., 1975, A seismic reflection method for solving engineering problems: *Journal of Geophysics*, v. 41, p. 267-284.
Schneider, W.A., Jr., K.A. Ranzinger, A.H. Balch, and C. Kruse, 1992, A dynamic programming approach to first arrival traveltime computation in media with arbitrarily distributed velocities: *Geophysics*, v. 57, p. 39-50.
Scott, J.H., 1977, SIPT–A seismic refraction inverse modeling program for timeshare terminal computer systems: U.S. Geological Survey Open-file Report 77-365.
Sheriff, R.E., 1991, Encyclopedic Dictionary of Exploration Geophysics: Society of Exploration Geophysicists, Tulsa.
Soske, J.L., 1954, The blind zone problem in engineering geophysics: *Geophysics*, v. 24, p. 359-365.
Steeples, D.W., and R.D. Miller, 1990, Seismic reflection methods applied to engineering, environmental, and groundwater problems: Soc. Explor. Geophys. Investigations in Geophysics no. 5, Stan H. Ward, ed., *Volume 1: Review and Tutorial,* p. 1-30.
Steinhart, J.S., and R.P. Meyer, 1961, Explosion studies of continental structure: Carnegie Institution of Washington Publication 622.
Stokoe II, K.H., S.G. Wright, J.A. Bay, and J.M. Roësset, 1994, Characterization of geotechnical sites by SASW method: in *Geophysical Characterization of Sites*, ISSMFE Technical Committee #10, ed. R.D. Woods, Oxford Publishers, New Delhi.
Xia, J., R.D. Miller, and C.B. Park, 1999, Estimation of near-surface velocity by inversion of Rayleigh waves: *Geophysics*, v. 64, p. 691-700.
Xia, J., R.D. Miller, C.B. Park, J.A. Hunter, J.B. Harris, and J. Ivanov, 2002, Comparing shear-wave velocity profiles from multichannel analysis of surface wave with borehole measurements: *Soil Dynamics and Earthquake Engineering*, v. 22, n. 3, p. 181-190.
Yilmaz, O., 1987, Seismic data processing; S.M. Doherty, ed.; *in* Series: Investigations in Geophysics, no. 2, E.B. Neitzel, series ed.: Soc. Explor. Geophys.
Zhang, J., and M.N. Toksoz, 1998, Nonlinear refraction traveltime tomography: *Geophysics*, v. 63, p. 1726-1737.